Separate universe approach to evaluate nonlinear matter power spectrum for nonflat ΛCDM model

Ryo Terasawa,[1,2,*] Ryuichi Takahashi,[3] Takahiro Nishimichi,[4,1] and Masahiro Takada[1]

[1]*Kavli Institute for the Physics and Mathematics of the Universe (WPI), The University of Tokyo Institutes for Advanced Study (UTIAS), The University of Tokyo, Chiba 277-8583, Japan*

[2]*Department of Physics, Graduate School of Science, The University of Tokyo, 7-3-1 Hongo, Bunkyo-ku, Tokyo 113-0033, Japan*

[3]*Faculty of Science and Technology, Hirosaki University, 3 Bunkyo-cho, Hirosaki, Aomori 036-8561, Japan*

[4]*Center for Gravitational Physics and Quantum Information, Yukawa Institute for Theoretical Physics, Kyoto University, Kyoto 606-8502, Japan*

(Received 3 June 2022; accepted 14 September 2022; published 7 October 2022)

The spatial curvature (Ω_K) of the Universe is one of the most fundamental quantities that could give a link to the early universe physics. In this paper we develop an approximate method to compute the nonlinear matter power spectrum, $P(k)$, for "nonflat" ΛCDM models using the separate universe (SU) ansatz which states that the effect of the curvature on structure formation is equivalent to that of background density fluctuation ($\delta_{\rm b}$) in a local volume in the "flat" ΛCDM model, via the specific mapping between the background cosmological parameters and redshifts in the nonflat and flat models. By utilizing the fact that the normalized response of $P(k)$ to $\delta_{\rm b}$ (equivalently Ω_K), which describes how the nonzero Ω_K alters $P(k)$ as a function of k, is well approximated by the response to the Hubble parameter h within the flat model, our method allows one to generalize the prediction of $P(k)$ for flat cosmologies via fitting formulas or emulators to that for nonflat cosmologies. We use N-body simulations for the nonflat ΛCDM models with $|\Omega_K| \leq 0.1$ to show that our method can predict $P(k)$ for nonflat models up to $k \simeq 6\ h{\rm Mpc}^{-1}$ in the redshift range $z \simeq [0, 1.5]$, to the fractional accuracy within ∼1% that roughly corresponds to requirements for weak lensing cosmology with upcoming surveys. We find that the emulators, those built for flat cosmologies such as `EuclidEmulator`, can predict the nonflat $P(k)$ with least degradation.

DOI: 10.1103/PhysRevD.106.083504

I. INTRODUCTION

The spatial curvature of the Universe (hereafter denoted as its contribution relative to the present-day critical density, Ω_K) is one of the most fundamental quantities in an isotropic and homogeneous universe in the context of general relativity [1]. The curvature also has a close connection to the physics of the early universe. An inflationary universe scenario predicts that the *apparent* curvature, inferred from an observable universe, should be close to a flat geometry ($\Omega_K \approx 0$), even if its exact value is nonzero [2,3]. If the universe arose form the decay of a false vacuum via quantum tunneling, as inspired by the landscape of string cosmology vacua, it leads to an open-geometry universe ($\Omega_K > 0$) [4,5]. Depending on the details of the early universe physics, the curvature can be large enough, such as $|\Omega_K| \simeq [10^{-4}, 10^{-2}]$, to be measurable by cosmological observations [6,7].[1] Therefore, an observational exploration of the curvature is an important direction to pursue with ongoing and upcoming cosmology datasets [e.g., [8,9]].

The curvature affects cosmological observables in two ways. First is its geometrical effect. The most promising observables are the baryon acoustic oscillations (BAO) imprinted onto the cosmic microwave background (CMB) anisotropies [10] and the distribution of galaxies [11]. Although the BAO scale [more exactly the sound horizon, as proposed by the pioneer works [12,13]] is set by the physics in the early universe, where the curvature's effect is negligible, the angular extent (and redshift difference) of the BAO scale, inferred from the CMB and galaxy

*ryo.terasawa@ipmu.jp

[1]If the curvature is as small as $|\Omega_K| \sim 10^{-5}$, we cannot distinguish between the global curvature and the primordial curvature "perturbations." Hence, the target goal for a hunt of the nonzero curvature is in the range $|\Omega_K| \gtrsim$ a few $\times\ 10^{-5}$.

observables, are determined by light propagation, which in turn allows us to infer the curvature parameter from the measured cosmological distances. Second, the curvature affects the growth of cosmic structure; since the time evolution of density fluctuation field arises from competing effects between the gravitational pulling force and the cosmic expansion, the curvature leaves a characteristic signature in the growth history of large scale structure via its effect on the cosmic expansion [e.g., [14]].

The geometrical constraint, inferred from the primary CMB anisotropy information of the *Planck* data [15], is given as $\Omega_K = -0.044^{+0.018}_{-0.015}$ (68% CL, *Planck* TT, TE, EE + lowE), implying a 2σ hint of the close geometry, although the constraint suffers from a severe parameter degeneracy (e.g., with the Hubble parameter h). The joint CMB and galaxy BAO measurements give the tightest constraint on Ω_K, consistent with a flat geometry: $\Omega_K = -0.0001 \pm 0.0018$ [16]. Ideally we want to use only galaxy BAO measurements at *multiple* redshifts to constrain the curvature, without employing the CMB prior on the BAO scale, to address whether the CMB and galaxy datasets have consistency within ΛCDM cosmologies, as motivated by the possible tensions between the CMB (early-time) and late-time universe datasets [e.g., see [17], for the recent review].

On the other hand, the growth constraint on the curvature is still in the early stage. Weak lensing and galaxy clustering, observed from wide-area galaxy surveys, are powerful methods to constrain cosmological parameters. However, most of the previous cosmological analyses assume a flat geometry and focus on the parameters to characterize the clustering amplitudes such as S_8 and $\Omega_{\rm m}$ [e.g., see [18], for the attempt to constrain Ω_K from the weak lensing data]. Although the curvature effect on the linear growth factor is accurately known, the linear-regime information is weaker than the BAO constraint. To obtain a tighter constraint on the curvature, we need an accurate model of the clustering observables that are applicable to the nonlinear regime. N-body and hydrodynamical simulations of cosmic structure formation are among the most powerful, accurate method for such a purpose. However, simulations are still expensive to construct the theoretical templates, especially in a multidimensional parameter space such as the vanilla ΛCDM model plus the curvature parameter. A more practical method at this stage is using the fitting formula or "emulation" based method [e.g., [19–30]]. However, such efforts developing the emulation method are usually done assuming flat-geometry cosmologies due to the computational expense.

Hence the purpose of this paper is to develop, as the first step, an approximate method for computing the nonlinear matter power spectrum, $P(k)$, for nonflat cosmologies, which is the fundamental quantity for weak lensing cosmology [31,32]. In fact the existing weak lensing measurements have been used to obtain tight constraints on the cosmological parameters [33–38]. The current and upcoming weak lensing surveys require a 1%-level or even better accuracy in the theoretical template of $P(k)$ up to $k \sim 1\ h{\rm Mpc}^{-1}$ in order not to have a significant bias in cosmological parameters such as dark energy parameters [39]. In this paper we employ the separate universe (SU) approach to study $P(k)$ for nonflat ΛCDM cosmologies. The SU ansatz states that the effect of the curvature on structure formation in a given nonflat ΛCDM model is equivalent to the effect of the long-wavelength (super-box) density fluctuation on the evolution of short-wavelength (sub-box) fluctuations in the counterpart flat-geometry ΛCDM model [40–44], where the cosmological parameters and redshifts in between the nonflat and flat models have to be mapped in the specific way. To study structure formation in the two mapped models, it is useful to use the "response" function of $P(k)$ which quantifies how $P(k)$ responds to the long-wavelength density fluctuation or equivalently the nonzero curvature, as a function of k. To develop our method, we further utilize the approximate identity that the response of $P(k)$ to the curvature, normalized relative to the response in the linear regime, is approximated by the normalized response of $P(k)$ to the Hubble parameter h [43]. By using the response to h, we can express $P(k)$ for a target nonflat ΛCDM model in terms of quantities for the corresponding flat ΛCDM model. That is, our method allows us to extend fitting formula or emulator, developed for flat-geometry cosmologies, to predicting $P(k)$ for nonflat model, which eases the computational cost for constructing the theoretical templates. We will validate our method using a set of N-body simulations for flat and nonflat ΛCDM models with $|\Omega_K| \leq 0.1$. We will also assess the performance of the publicly available emulator for computing $P(k)$ for nonflat models.

This paper is organized as follows. In Sec. II we first review the SU approach and then describe our approximate method for computing the nonlinear matter power spectrum for nonflat ΛCDM models. In Sec. III we describe details of N-body simulations for flat and nonflat ΛCDM models. In Sec. IV we present the main results of this paper. We first validate the approximation for the normalized growth response as we described above, and then show the accuracy of our method for predicting the nonlinear matter power spectrum for nonflat ΛCDM model. Section V is devoted to discussion and conclusion. In Appendix we give justification of our method based on the halo model. Throughout this paper we use notations $\Omega_{\rm m}$ and Ω_Λ to denote the density parameters for nonrelativistic matter and the cosmological constant, respectively.

II. SU ESTIMATOR OF $P(k)$ FOR NONFLAT ΛCDM MODEL

In this section we develop a method to compute $P(k)$ for nonflat ΛCDM model, from quantities for the corresponding flat ΛCDM model based on the SU approach [40–47].

A. Preliminary

Before going to our method we would like to introduce a motivation to use the SU approach. One might naively think that we can use a Taylor expansion of $P(k,z;\Omega_K)$ treating Ω_K as an expansion parameter; $P(k,z;\Omega_K) \approx P(k,z)|_{\Omega_K=0} + (\partial P/\partial\Omega_K)|_{\Omega_K=0}\Omega_K$, where $P(k,z)|_{\Omega_K=0}$ is the power spectrum for a flat model. However, there is no unique way to define this partial derivative operation. In particular, we have to satisfy the identity $\Omega_K = 1-(\Omega_{\rm m}+\Omega_\Lambda)$ and vary cosmological parameters other than Ω_K simultaneously. In addition, there is ambiguity in how the time variable is matched between the flat and curved models. The simplest examples are to match the redshift, or the physical time, while these might not be optimal. As a working example, we utilize the SU approach for connecting the power spectra for nonflat and flat ΛCDM models.

B. SU approach for $P(k)$

The effect of curvature (Ω_K) on structure formation appears only in the late universe. In other words, the curvature does not affect structure formation in the early universe such as CMB physics (as long as the curvature parameter is small as indicated by current observations). Hence throughout this paper we employ models where structure formation in the early universe is identical. This is equivalent to keeping the parameters,

$$\{\omega_{\rm c},\omega_{\rm b},A_s,n_s\}, \tag{1}$$

fixed, where $\omega_{\rm c}(\equiv\Omega_{\rm c}h^2)$ and $\omega_{\rm b}(\equiv\Omega_{\rm b}h^2)$ are the physical density parameters of CDM and baryon, respectively, and A_s and n_s are the amplitude (at the pivot scale $k_{\rm pivot} = 0.05\ {\rm Mpc}^{-1}$) and the spectral tilt of the power spectrum of primordial curvature perturbations. Note that, when we include massive neutrinos, throughout this paper we fix the sum of neutrino masses so that the early universe physics remains unchanged [e.g., see Refs. [26,48], for the method]. The linear matter power spectrum is given as

$$P^{\rm L}(k,z) = \left(\frac{D(z)}{D(z_i)}\right)^2 P^{\rm L}(k,z_i), \tag{2}$$

where z_i is the initial redshift in the linear regime satisfying $z_i \gg 1$ yet well after the matter-radiation equality such that residual perturbations in radiation do not play a role and $D(z)$ is the linear growth factor.[2] The superscript "L" stands for the linear-theory quantities. In our method, we keep the linear power spectrum at z_i, $P^{\rm L}(k,z_i)$, fixed.

Let us consider a nonflat ΛCDM model, denoted as Ω_K-ΛCDM, as a target model for which we want to estimate the nonlinear matter power spectrum at z in the late universe. The background expansion for this target Ω_K-ΛCDM model is specified by

$$\Omega_K\text{-}\Lambda{\rm CDM}:\{\Omega_K,h\}. \tag{3}$$

Once the parameters in Eqs. (1) and (3) are specified, the other parameters in Ω_K-ΛCDM cosmology are fully fixed; $\Omega_{\rm m} = (\omega_{\rm c}+\omega_{\rm b})/h^2$ for the density parameter for matter, and $\Omega_\Lambda = 1-\Omega_K-\Omega_{\rm m}$ for the cosmological constant. The following discussion can be applied only to ΛCDM model, so we do not consider a model with dynamical dark energy [e.g., see [49], for discussion on the SU approach for dynamical dark energy model].

The SU approach gives a mapping between nonflat ΛCDM and flat ΛCDM models by assigning the degree of Ω_K in the former cosmology to the background density fluctuation, denoted as $\delta_{\rm b}(t)$, in the latter flat ΛCDM model. We call the "fake" flat-ΛCDM model as fΛCDM model. Following Li *et al.* [42], in the SU approach the physical matter densities in the two models are related as

$$\bar\rho_{\rm m}(t) = \bar\rho_{{\rm m}f}(t)[1+\delta_{\rm b}(t)]. \tag{4}$$

Here and throughout this paper we assume $\delta_{\rm b}(t)$ evolves according to the linear growth factor $D_f(t)$ as $\delta_{\rm b}(t) \propto D_f(t)$, and we denote quantities in the fΛCDM model by subscript "f." Equation (4) gives

$$\frac{\Omega_{\rm m}h^2}{a(t)^3} = \frac{\Omega_{{\rm m}f}h_f^2}{a_f(t)^3}[1+\delta_{\rm b}(t)], \tag{5}$$

where $\Omega_{\rm m}$ and $h(\Omega_{{\rm m}f}$ and $h_f)$ are defined at $a=1$ ($a_f=1$). Note that $a=1$ and $a_f=1$ correspond to different cosmic times for $\delta_{\rm b}\neq 0$. We set a_f to agree with a at very high redshift in the early universe, where $|\delta_{\rm b}(t)| \ll 1$, which leads to $\Omega_{{\rm m}f}h_f^2 = \Omega_{\rm m}h^2$. This condition gives a mapping between the scale factors:

$$a_f(t)[1+\delta_{\rm b}(t)]^{-1/3} = a(t). \tag{6}$$

Here we assume that Ω_K-ΛCDM universe and the fake flat universe share a common cosmic time, hence the mapping between quantities in the two universes should be found at the same cosmic time (t). Equation (6) allows us to find the scale factor $a_f(t)$ in fΛCDM model, corresponding to $a(t)$ in Ω_K-ΛCDM model, at the same cosmic time. Equivalently we can derive the mapping for redshift as $(1+z_f)[1+\delta_{\rm b}(z_f)]^{1/3} = 1+z$. The redshift z_f in the fake

[2] In reality, at the typical starting redshifts of simulations, the residual radiation perturbations are not completely negligible, leaving scale-dependent corrections to the linear growth factor. Here we assume a situation that, as usually done when setting up the initial conditions of an N-body simulation, one can first evolve the baryon and CDM perturbations until today (well after the two components catch up with each other), and then trace back the "single-fluid" perturbation to the initial redshift by using the linear growth factor for a given cosmological model.

universe corresponding to the target redshift z can be found by solving numerically Eq. (6).

The difference of the first Friedmann equations of Ω_K-ΛCDM model and fΛCDM model yields the equation for the curvature. Evaluating this at an early time t_i gives

$$\frac{\delta_{\rm b}(t_i)}{a_f(t_i)} = -\frac{3\Omega_K}{5\Omega_{\rm m}}. \tag{7}$$

Please see Ref. [44] (also see Ref. [42]) for a more complete derivation. This can be rewritten as

$$\frac{\delta_{\rm b}(t)}{D_f(t)} = -\frac{3\Omega_K}{5\Omega_{\rm m}}, \tag{8}$$

where the linear growth factor is normalized as $D_f(t_i) = a_f(t_i)$. We note that there is a one-to-one correspondence between Ω_K and $\delta_{\rm b}(t)$. Since the expansion history of the target Ω_K-ΛCDM cosmology is different from the fΛCDM cosmology, we expect that the parameter h_f is also modified by $\delta_{\rm b}$. If we set $h_f \equiv h(1+\delta_h)$, the condition $\Omega_{{\rm m}f}h_f^2 = \Omega_{\rm m}h^2$ yields a mapping for $\Omega_{{\rm m}f}$ as

$$\Omega_{{\rm m}f} = \Omega_{\rm m}(1+\delta_h)^{-2}. \tag{9}$$

Since dark energy is assumed to be a cosmological constant, there is no perturbation in the dark energy induced by $\delta_{\rm b}$. Hence Ω_K-ΛCDM model and fΛCDM model share the same ρ_Λ, which leads

$$\Omega_{\Lambda f} = \Omega_\Lambda(1+\delta_h)^{-2}. \tag{10}$$

The flat-geometry condition for fΛCDM model, i.e., $\Omega_{Kf} = 0$ (or $\Omega_{{\rm m}f} + \Omega_{\Lambda f} = 1$), gives the following identity:

$$\delta_h = (1-\Omega_K)^{1/2} - 1. \tag{11}$$

These results indicate that for linear matter power spectrum fixed by Eqs. (1) and (2), the remaining two degrees of freedom, Ω_K and h are fully specified by $\delta_{\rm b}$ [Eqs. (8) and (11)] in the SU approach. Conversely, we can recast the effect of Ω_K on structure formation as the effect of $\delta_{\rm b}$ on a local volume in a fake flat universe.

According to the SU approach [42,43], the power spectrum at z in Ω_K-ΛCDM model can be approximated by the power spectrum at z_f in fΛCDM model as

$$\begin{aligned}\tilde{P}(k,z;\Omega_K) &\simeq P_f(k,z_f;\delta_{\rm b}) \\ &\simeq P_f(k,z_f)|_{\delta_{\rm b}=0} + \left.\frac{\partial P_f(k,z_f;\delta_{\rm b})}{\partial\delta_{\rm b}}\right|_{\delta_{\rm b}=0}\delta_{\rm b} \\ &= P_f(k,z_f)|_{\delta_{\rm b}=0}\left[1+\left.\frac{\partial \ln P_f(k,z_f;\delta_{\rm b})}{\partial\delta_{\rm b}}\right|_{\delta_{\rm b}=0}\delta_{\rm b}\right],\end{aligned} \tag{12}$$

where $\delta_{\rm b} \equiv \delta_{\rm b}(z_f)$. The relation between z and z_f is given by Eq. (6). We often call $\partial P_f(k)/\partial\delta_{\rm b}$ the growth "response" which describes how the power spectrum at k responds to the long-wavelength mode $\delta_{\rm b}$ in fΛCDM model. We have put the tilde symbol ~ in $\tilde{P}(k,z;\Omega_K)$ to explicitly denote that $\tilde{P}$ is an "estimator" of the nonlinear matter power spectrum for Ω_K-ΛCDM model. Note that we need to compute these quantities at k in the comoving wave numbers of the target Ω_K-ΛCDM model, so we need not include the dilation effect, i.e., the mapping between comoving wave numbers in between the nonflat and flat models, differently from the method in Ref. [42].

1. h response

So far, we have revisited the basic equations of the SU approach. As explained earlier, the SU response is not the unique way to induce perturbations to a flat fiducial cosmology for fixed values of parameters in Eq. (1), that fully specify the linear matter power spectrum. Here we consider a simple example of perturbing h while the spatial flatness is kept.

For convenience of our discussion, we introduce the normalized response, from Eq. (12), as

$$\tilde{P}(k,z;\Omega_K) \simeq P_f(k,z_f)\left[1+\frac{26}{21}T_{\delta_{\rm b}}(k,z_f)\delta_{\rm b}(z_f)\right], \tag{13}$$

with

$$T_{\delta_{\rm b}}(k,z_f) \equiv \left[2\frac{\partial \ln D_f(z_f)}{\partial\delta_{\rm b}}\right]^{-1}\left.\frac{\partial \ln P_f(k,z_f;\delta_{\rm b})}{\partial\delta_{\rm b}}\right|_{\delta_{\rm b}=0}. \tag{14}$$

The normalized response has an asymptotic behavior of $T_{\delta_{\rm b}} \to 1$ at the linear limit $k \to 0$, because $P_f(k) \propto (D_f)^2P^L(k,z_i)$ in such linear regime [see Eq. (2)]. The coefficient, 26/21, in the second term in the square bracket on the rhs comes from the linear limit of $k \to 0$ [40,41].

As we will show below or discussed in Ref. [43] (around Fig. 6 in the paper), we propose that the power spectrum for the target Ω_K-ΛCDM model is well approximated by replacing the normalized response to $\delta_{\rm b}$ with the normalized response with respect to h within the flat model:

$$\tilde{P}(k,z;\Omega_K) \simeq P_f(k,z_f)\left[1+\frac{26}{21}T_h(k,z_f)\delta_{\rm b}(z_f)\right], \tag{15}$$

with

$$T_h(k,z_f) \equiv \left[2\frac{\partial \ln D_f(z_f)}{\partial h_f}\right]^{-1}\frac{\partial \ln P_f(k,z_f)}{\partial h_f}, \tag{16}$$

where the partial derivative $\partial/\partial h_f$ is the derivative with respect to h_f, while keeping the other cosmological parameters [Eq. (1)] fixed to their fiducial values; more

explicitly we vary h with keeping $\Omega_{\rm m}h^2$ fixed, and accordingly we have to change $\Omega_{\rm m}$ (and Ω_Λ from the identity $\Omega_\Lambda = 1 - \Omega_{\rm m}$ for flat models). Here we defined the normalized response satisfying $T_h(k) \to 1$ at $k \to 0$. If $T_{\delta_{\rm b}}(k, z_f) \simeq T_h(k, z_f)$ for an input set of k and z_f as we will show below, we can use Eq. (15) to approximate the nonlinear matter power spectrum at z for the target Ω_K-ΛCDM model.

C. Linear limit

The SU picture has an analogy with the spherical collapse model [50–52], where a spherical tophat over- or underdensity fluctuation is embedded into the FRW homogeneous background and then the time-evolution of the tophat interior density can be fully tracked up to the fully nonlinear regime. As described in Wagner *et al.* [44], we can derive a mapping between the full growth factor of such a spherical tophat density and the linearly extrapolated density fluctuation $\delta_{\rm b}$ up to the full order of $\delta_{\rm b}$. In the SU setup this is equivalent to expressing the growth factor of density fluctuations in a local volume with $\delta_{\rm b}$, denoted as $\tilde{D}_f(z_f; \delta_{\rm b})$, in terms of the growth factor in the background of the fake universe [from Eq. (C.17) in Ref. [53]]:

$$\tilde{D}_f(z_f; \delta_{\rm b}) \simeq D_f(z_f)\left[1 + \frac{13}{21}\delta_{\rm b} + \frac{71}{189}\delta_{\rm b}^2 + \frac{29609}{130977}\delta_{\rm b}^3\right], \tag{17}$$

where $\delta_{\rm b} = \delta_{\rm b}(z_f)$. Comparison of Eqs. (13) and (17) clarifies that the expression of Eq. (13) corresponds to the linear-order expansion of the linear growth factor in terms of $\delta_{\rm b}$, because $P_f(k, z_f; \delta_{\rm b}) \propto \tilde{D}_f(z_f, \delta_{\rm b})^2$ at the linear limit. The coefficient $26/21$ on the right-hand side (rhs) in Eq. (15) comes from the first-order expansion of the linear growth factor in Eq. (17): $(\tilde{D}_f/D_f)^2 \simeq 1 + (26/21)\delta_{\rm b}$. Because we know the exact mapping between the linear growth factors in the Ω_K-ΛCDM and fΛCDM models, we can fully account for the mapping at the linear limit. We will later include this linear-limit correction.

Figure 1 shows the accuracy of the approximation of the growth factor, $[\tilde{D}_f(z_f; \delta_{\rm b})/D(z; \Omega_K)]^2$ when truncated at some finite order in $\delta_{\rm b}$, as a function of the input Ω_K in the x-axis, where $D(z; \Omega_K)$ is the true growth factor for Ω_K-ΛCDM model. The value of $\delta_{\rm b}$ is specified by the input Ω_K in the x-axis, from Eq. (8). The dashed, solid, and dotted curves show the ratio when including only the zeroth term, or up to the 1st or 2nd term, respectively, in the square bracket of the rhs of Eq. (17). The 1st-order expansion (solid curve) corresponds to the approximation of the power spectrum, $\tilde{P}(k, z; \Omega_K)/P(k, z; \Omega_K)$ [Eq. (13)] at linear limit ($k \to 0$). Encouragingly, the 1st-order approximation (solid curve) is accurate to within about 2% in the fractional amplitude for the range of $|\Omega_K| < 0.1$, which is very broad compared to the current constraint, $|\Omega_K| < 0.1$ (2σ level) from the *Planck* CMB data alone [15]. Note that, if we do not take into account the mapping of redshifts ($z_f \leftrightarrow z$) or we forcibly use the power spectrum at z in the fake universe, the accuracy of the 1st-order approximation is significantly degraded. We also note that the results are similar for other redshifts, but have better accuracy with the increase of redshift.

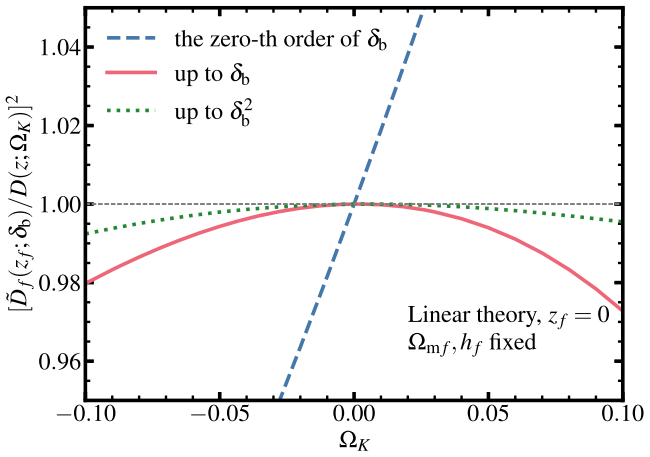

FIG. 1. An accuracy of the approximation that gives the growth factor for Ω_K-ΛCDM model in terms of the growth factor for the corresponding flat ΛCDM model and the Taylor expansion of $\delta_{\rm b}$ in the SU approach [Eq. (17)]. Here $\delta_{\rm b}$ is related to the curvature parameter Ω_K, in the x-axis, of each Ω_K-ΛCDM model, via Eq. (8). Note that we consider $z_f = 0$ and fixed the other cosmological parameters $\Omega_{{\rm m}f}$ and h_f as $\Omega_{{\rm m}f} = 0.3156$ and $h_f = 0.6727$ in the flat ΛCDM model. Here we assess $[\tilde{D}_f(z_f; \delta_{\rm b})/D(z; \Omega_K)]^2$, where $D(z; \Omega_K)$ is the true growth factor for each Ω_K-ΛCDM model, because the ratio corresponds to the linear limit of the approximation of matter power spectrum we study in this paper. The dashed, solid, and dotted curves denote the results for the approximations obtained when including the zeroth-, first-, or second-order expansion of $\delta_{\rm b}$ in Eq. (17).

D. Summary: Estimator of $P(k)$ for nonflat ΛCDM

By combining Eqs. (15) and (17), we propose the following approximation to compute the nonlinear matter power spectrum at z for Ω_K-ΛCDM model that is specified by the parameters $(\Omega_K, \Omega_{\rm m}, h)$:

$$\tilde{P}(k, z) \simeq P_f(k, z_f)\left(\frac{D(z)}{D_f(z_f)}\right)^2 \times \left[1 + \frac{26}{21}\{T_h(k, z_f) - 1\}\delta_{\rm b}(z_f)\right], \tag{18}$$

with

$$\delta_{\rm b}(z_f) = -D_f(z_f)\frac{3\Omega_K}{5\Omega_{\rm m}},$$
$$(1+z_f)[1+\delta_{\rm b}(z_f)]^{1/3} = 1+z,$$
$$T_h(k,z_f) = \left[2\frac{\partial \ln D_f(z_f)}{\partial h_f}\right]^{-1}\frac{\partial \ln P_f(k,z_f)}{\partial h_f}. \quad (19)$$

Note that the parameters $(h_f, \Omega_{{\rm m}f}, \Omega_{\Lambda f})$ for $f\Lambda$CDM model are given by Eqs. (9), (10), and (11), and the other cosmological parameters to specify the transfer function and the primordial perturbations $(\omega_{\rm c}, \omega_{\rm b}, A_s, n_s)$ are kept fixed in the Ω_K-ΛCDM and $f\Lambda$CDM models.

We employed the modification of Eq. (18) from Eq. (15) to fully take into account the modification in the linear growth factor up to the full order of $\delta_{\rm b}$; Eq. (18), by design, reproduces the underlying true power spectrum for Ω_K-ΛCDM model at the linear limit, i.e., $\tilde{P}(k,z) = P(k,z)$ at $k \to 0$ [also from Eq. (2)].

All the terms on the rhs of Eq. (18), except for $D(z)$, are given by quantities for the flat-geometry $f\Lambda$CDM model, which are specified by the cosmological parameters of Ω_K-ΛCDM model. That is, if Eq. (18) is a good approximation, we can evaluate the nonlinear matter power spectrum for an arbitrary Ω_K-ΛCDM model from the quantities for the counterpart flat model in the SU approach. For example, if we use the fitting formulas or emulators of nonlinear matter power spectrum calibrated for flat ΛCDM cosmologies, we can compute the nonlinear matter power spectrum for the target Ω_K-ΛCDM model. This would be a useful approximation, and we will below give validation of our method, and quantify the accuracy of our method.

III. SIMULATION DATA

A. *N*-body simulations

To validate our method [Eq. (18)], we use cosmological N-body simulations. Our simulations follow the method in Nishimichi *et al.* [26], and we here give a brief summary of the simulations used in this paper.

We use GADGET-2 [54] to carry out N-body simulation for a given cosmological model. The initial conditions are set up at redshift $z_i = 59$ using the second-order Lagrangian perturbation theory [55,56] implemented by Nishimichi *et al.* [57] and then parallelized in Valageas and Nishimichi [58]. We use the public code CAMB [59] to compute the transfer function for a given model, which is used to compute the input linear power spectrum. For all simulations in this paper, we use the same simulation box size in Gpc (i.e., without h in the units) and the same number of particles: $L = 1\ h_f^{-1}{\rm Gpc} \simeq 1.49$ Gpc (without h in units) and $N_p = 2048^3$, which correspond to the particle Nyquist wave number, $k = 6.4\ h_f{\rm Mpc}^{-1}$. In the following we will show the results at wave numbers smaller than this Nyquist wave number.

In this paper we use simulations for five different cosmological models, denoted as "fiducial" flat ΛCDM, "Ω_K-ΛCDM1," "Ω_K-ΛCDM2," "Ω_K-ΛCDM3," and "h-ΛCDM" models, respectively, as given in Table I. Here the cosmological parameters for the "fiducial" model are chosen to be consistent with those for the *Planck* 2015

TABLE I. Details of N-body simulations for different cosmological models. The columns "Ω_K" and "h" give their values of the curvature parameter and Hubble parameter that are employed in each simulation, while we fix other cosmological parameters $\{\omega_{\rm c}, \omega_{\rm b}, A_s, n_s\}$, which are needed to specify the linear power spectrum for the initial conditions, to the values for the fiducial *Planck* cosmology (see text for details). $\Omega_{\rm m}$ and Ω_Λ are specified by a given set of Ω_K and h, because we keep $\Omega_{\rm m}h^2$ fixed and $\Omega_\Lambda = 1 - \Omega_{\rm m} - \Omega_{\rm K}$. The column "$N_{\rm real}$" denotes the number of realizations, with different initial seeds, used for each model. The column "Angulo-Pontzen" gives whether or not we employ the "paired-and-fixed" method in [61] to reduce the sample variance effect in small k bins for the power spectrum measurement: we adopt the method for "Yes," while not for "No." For the paired-and-fixed method, it uses the paired (2) simulations by design (see text for details). The column "redshift (z)" gives the redshifts of simulation outputs: for Ω_K-ΛCDM model, we properly choose the redshifts corresponding to the same cosmic time for each of redshifts, $z = \{0.0, 0.549, 1.025, 1.476\}$ in the "fiducial" model in the SU approach (see around Eq. (6) in Sec. II B). All the simulations are done in the fixed comoving box size without h in its units, i.e., $L \simeq 1.49$ Gpc (corresponding to $1\ h_f^{-1}$Gpc for the fiducial model) and with the same particle number, i.e., $N_p = 2048^3$.

Name	Ω_K	h	$N_{\rm real}$	Angulo-Pontzen	Redshift (z)
Flat (fiducial)	0	0.6727	2	Yes.	$\{0.0, 0.549, 1.025, 1.476\}$
Ω_K-ΛCDM1	0.00663	0.6749	10	No.	$\{-0.0033, 0.544, 1.018, 1.467\}$
	−0.00672	0.6705	10	No.	$\{0.0033, 0.554, 1.031, 1.484\}$
Ω_K-ΛCDM2	0.05	0.6902	2	Yes.	$\{-0.027, 0.518, 0.992, 1.443\}$
	−0.05	0.6565	2	Yes.	$\{0.023, 0.576, 1.053, 1.505\}$
Ω_K-ΛCDM3	0.1	0.7091	2	Yes.	$\{-0.059, 0.482, 0.955, 1.405\}$
	−0.1	0.6414	2	Yes.	$\{0.043, 0.600, 1.079, 1.531\}$
h-ΛCDM	0	0.6927	10	No.	$\{0.0, 0.549, 1.025, 1.476\}$
	0	0.6527	10	No.	$\{0.0, 0.549, 1.025, 1.476\}$

best-fit cosmology [60]. The cosmological parameters for each of the nonflat cosmological models are chosen so that it has the fiducial ΛCDM model as the "fake" flat ΛCDM model in the SU approach. We use paired simulations for "Ω_K-ΛCDM1" model to compute the power spectrum response with respect to $\delta_{\rm b}$ ($T_{\delta_{\rm b}}$), where the curvature parameters are specified by $\delta_{\rm b} = \pm 0.01$ at $z_f = 0$. The "h-ΛCDM" model is for computing the response with respect to h (T_h): here, we chose a step size of $\delta h = \pm 0.02$ for the numerical derivative. Note that the setup of these simulations is designed to compute the "growth" response by taking the numerical derivative at fixed comoving wave numbers k [see Sec. III B in Ref. [42]]. We also use the simulations for nonflat ΛCDM models with $\Omega_K = \pm 0.05$ or ± 0.1, named as "Ω_K-ΛCDM2" and "Ω_K-ΛCDM3," to assess how our method can approximate the matter power spectrum for nonflat models.

Table I gives the values of Ω_K and h, and we use the fixed values of other cosmological parameters, given as $(\omega_{\rm c}, \omega_{\rm b}, A_s, n_s) = (0.1198, 0.02225, 2.2065 \times 10^{-9}, 0.9645)$, which specify the transfer function and the primordial power spectrum, or equivalently the linear matter power spectrum. Note that we also include the effect of massive neutrinos on the linear matter power spectrum, assuming $\Omega_\nu h^2 = 0.00064$ corresponding to $m_{\nu,\rm tot} = 0.06$ eV, the lower limit inferred from the oscillation experiments [see Ref. [26], for details]. Hence the physical density parameter of total matter is $\Omega_{\rm m} h^2 = \omega_{\rm c} + \omega_{\rm b} + \omega_\nu$. Note that $\Omega_{\rm m}$ and Ω_Λ are specified by a given set of the parameters for each model: $\Omega_{\rm m} = \Omega_{{\rm m}f} h_f^2 / h^2$ and $\Omega_K = 1 - (\Omega_{\rm m} + \Omega_\Lambda)$. For each model, we use the outputs at 4 redshifts, $z_f \simeq 0$, 0.55, 1.03, and 1.48. Since the fiducial flat ΛCDM model is the fake flat model in the SU method, each redshift for the fiducial flat model corresponds to a slightly different redshift in each nonflat model, which is computed from Eq. (6).

Note that all the N-body simulations for different cosmological models are designed to have the fixed mass resolution, $m_p \simeq 1.52 \times 10^{10}\ M_\odot$ (in units without h). Hence the comoving mass density in the N-body box is kept fixed: $\bar{\rho}_{\rm m0} = N_p m_p / V_{\rm com} \simeq 3.96 \times 10^{11}\ M_\odot {\rm Mpc}^{-3}$. We utilize this fact to define a sample of halos in the same mass bins, in units of $M_\odot$, for all the cosmological models. This makes it easier to compute the response of halo mass function with respect to $\delta_{\rm b}$ or h, which is used to study the power spectrum responses based on the halo model (see Appendix).

Furthermore, we use simulations that are run using the "paired-and-fixed" method in Angulo and Pontzen [61], where the initial density field in each Fourier mode is generated from the fixed amplitude of the power spectrum $\sqrt{P(k)}$ and the paired simulations with reverse phases, i.e., $\delta_{\mathbf{k}}$ and $-\delta_{\mathbf{k}}$, are run. The mean power spectrum of the paired runs fairly well reproduces the ensemble average of many realizations even in the nonlinear regime [61,62]. The paired-and-fixed simulations allow us to significantly reduce the sample variance in the power spectrum estimation. The column "Angulo-Pontzen" in Table I denotes whether we use the paired-and-fixed simulations. For the paired-and-fixed simulations, "2" on the column $N_{\rm real}$ denotes one pair of the paired-and-fixed simulations.

B. Measurements of power spectrum and growth response

To calculate the power spectrum from each simulation output, we assign the particles on 2048^3 grids using the cloud-in-cells (CIC) method [63] to obtain the density field. After performing the Fourier transform, we correct for the window function of CIC following the method described in Takahashi *et al.* [23]. In addition, to evaluate the power spectrum at small scales accurately, we fold the particle positions into a smaller box by replacing $\mathbf{x} \to \mathbf{x}\%(L/10^n)$, where the operation $a\%b$ stands for the reminder of the division of a by b. This procedure leads to effectively 10^n times higher resolution. Here we adopt $n = 0, 1$. We use the density fluctuation $\delta_{\mathbf{k}}$ up to half the Nyquist frequency determined by the box size $L/10^n$ with the grid number, and we will show the results at wave numbers smaller than $k = 6.4\ h_f {\rm Mpc}^{-1}$.

Since we use the fixed box size and the same particle number, we use the same k binning to estimate the average of $|\delta_{\mathbf{k}}|^2$ in each k bin to estimate the band power. We then use the two-side numerical derivative method to compute the power spectrum responses. To reduce statistical stochasticity (or sample variance), we employ the same initial seeds as those for the "fiducial" model. The column "$N_{\rm real}$" in Table I denotes the number of realizations for paired simulations, where each pair uses the same initial seeds. For Ω_K-ΛCDM1 and h-ΛCDM models, we further run 9 paired simulations to estimate the statistical scatters; hence we use 10 paired simulations in total to estimate the power spectrum responses at each redshift, $T_{\delta_{\rm b}}(k, z_f)$ and $T_h(k, z_f)$.

IV. RESULTS

A. Power spectrum responses

In Fig. 2 we study the normalized growth responses of matter power spectrum, $T_{\delta_{\rm b}}(k)$ and $T_h(k)$, at the four redshifts, which are computed from the N-body simulations for Ω_K-ΛCDM1 and h-ΛCDM models, respectively, in Table I. It is clear that the approximate identity of $T_{\delta_{\rm b}} \approx T_h$ holds over the range of scales and for all the redshifts. To be more precise, the two responses agree with each other to within 2(16)% in the fractional amplitudes for $k \lesssim 1(6.4)\ h_f {\rm Mpc}^{-1}$. Our results confirm the result of Li *et al.* [43] (see Fig. 6 in the paper). However, a closer look of Fig. 2 reveals a slight discrepancy at $k \gtrsim 1\ h_f {\rm Mpc}^{-1}$. As we showed in Appendix, the responses at these small scales

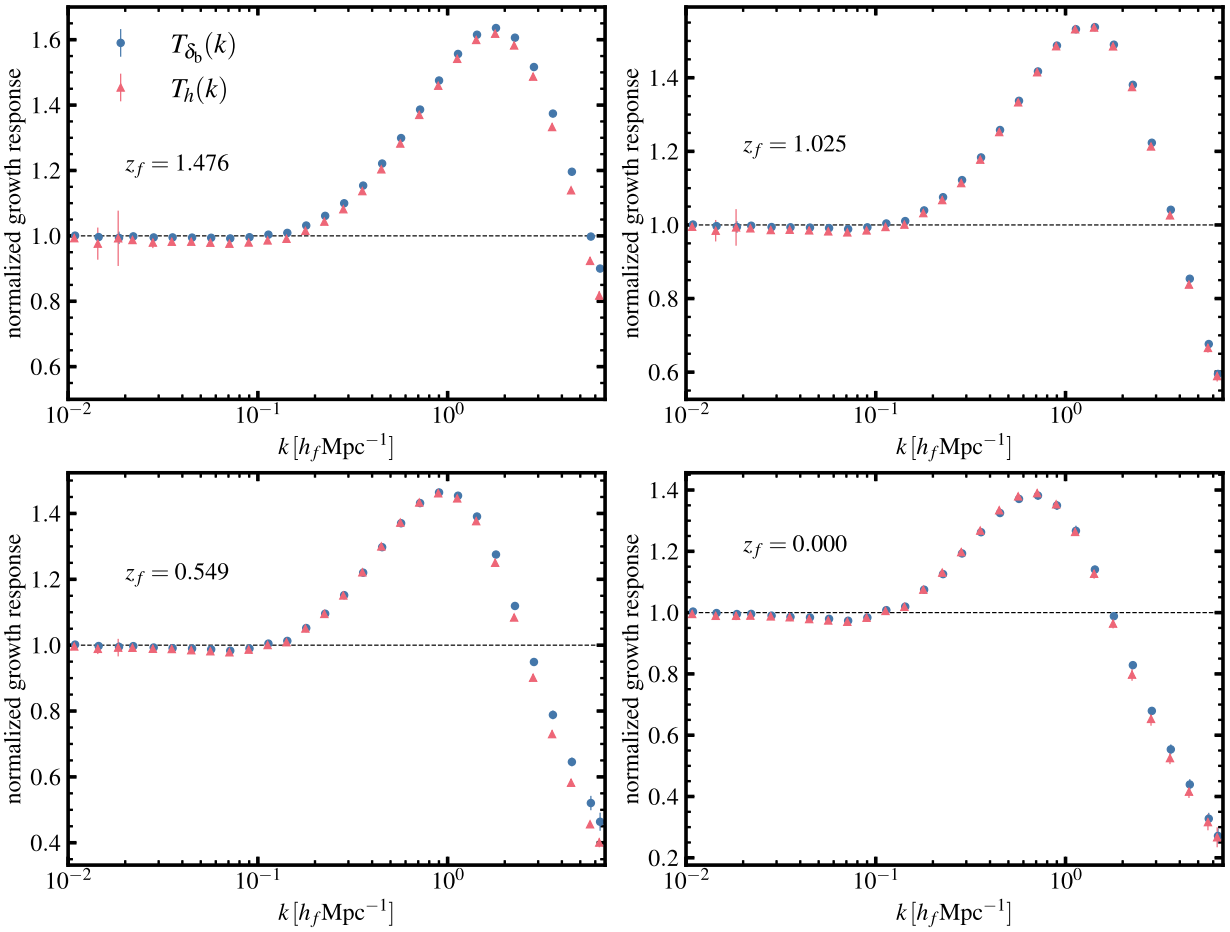

FIG. 2. Normalized growth response of matter power spectrum with respect to δ_b and h, $T_{\delta_b}(k)$ and $T_h(k)$, at the four redshifts as denoted by the legend in each panel. The horizontal line denotes the linear limit: $T_{\delta_b}, T_h = 1$. We use the 10 paired simulations for Ω_K-ΛCDM1 and h-ΛCDM models in Table I to compute these responses. The circle or triangle symbols denote the mean of T_{δ_b} or T_h in each k bin, and the error bars (although not visible in some k bins) denote the statistical errors for simulation box with side length $L = 1\ h_f^{-1}$Gpc, which are estimated from the standard deviations among the 10 paired simulations. Note that the range of y-axis is different in different panels.

are mainly from modifications in the mass density profiles of halos. Hence we conclude that the identity of $T_{\delta_b} \approx T_h$ is not exact, but approximately valid for models around the fiducial ΛCDM models we consider.

Since δ_b and h are varied at fixed initial power spectrum, their impact on the power spectrum in the linear regime at a fixed comoving scale comes solely from changing the linear growth factor D. Since we normalize the response to account for this linear dependence on D, the data points converge to unity at the low-k limit by design.

For the quasi nonlinear regime, the perturbation theory of structure formation predicts that the higher-order loop corrections to the power spectrum are well approximated by a separable form in terms of time and scale: an exact result for the Einstein-de Sitter (EdS) cosmology, which is usually generalized to ΛCDM cosmology by replacing the scale factor a with the linear growth factor D. Possible corrections to this arising from the nonseparability is known to have a weak dependence on $\Omega_m(z)$, and this can be usually ignored in the modeling of mildly nonlinear regime [64–67]. Under this approximation, the nonlinear power spectrum is fully specified by its linear counterpart evaluated at the same redshift. Therefore the perturbation theory also predicts that $T_{\delta_b} \approx T_h$ should be valid due to the matched shape of the linear power spectrum.

The agreement $T_{\delta_b} \approx T_h$ in the nonlinear regime suggests that nonlinear matter power spectrum is approximately given by a functional form of the input linear power spectrum, $\Delta^2_{\rm NL}(k) = F_{\rm NL}[\Delta^2_{\rm L}(k)]$ $(\Delta^2 \equiv k^3P(k)/2\pi^2)$, as implied by the stable clustering ansatz for a CDM model [19,68–71]. If the ansatz holds, the identity $T_{\delta_b} = T_h$ holds exactly. In Appendix, we also show that the approximation $T_{\delta_b} \approx T_h$ can be found from the halo model picture, which is derived using the growth responses of the halo mass function and the halo mass density profile to δ_b and h that are estimated from N-body simulations. Thus the results of

Fig. 2 suggest that the stable clustering ansatz is approximately valid.

Before proceeding, we comment on the normalized growth response to the primordial power spectrum amplitude A_s: $T_{A_s}(k,z_f) \equiv [2\partial \ln D_f(z_f)/\partial A_s]^{-1}\partial \ln P_f(k,z_f)/\partial A_s$. A change in A_s does not alter the shape of the linear matter power spectrum. If the stable clustering is exact, one would expect $T_{A_s} = T_{\delta_b}$. However, as shown in Fig. 6 of Li *et al.* [43] [also see [53]], T_{A_s} shows a sizable discrepancy from T_{δ_b} (or T_h) at $k \gtrsim 0.1\ h_f\mathrm{Mpc}^{-1}$. This means that a change in A_s leads to a larger change in the transition scale ($k_{\rm NL}$) between the linear and nonlinear regimes, or a larger change in the halo profile (e.g., the halo concentration). Hence, we again stress that $T_{\delta_b}(k) \approx T_h(k)$ is an approximate identity around the ΛCDM model.

In Fig. 3 we assess the accuracy of the publicly available fitting formula of $P(k)$ for predicting the normalized growth response. Here we employ the two versions of `Halofit` in Smith *et al.* [20] (Smith + 03) and Takahashi *et al.* [23] (Takahashi + 12), respectively, and the `HMcode` in Mead *et al.* [28] (Mead + 20). All the fitting formulas are primarily functionals of the linear power spectrum at the target redshift (although each formula includes terms that have an extra dependence on cosmological parameters). Among these fitting formulas, only Smith + 03 `Halofit` was calibrated against N-body simulations for models including nonflat CDM model. Note that we here compute

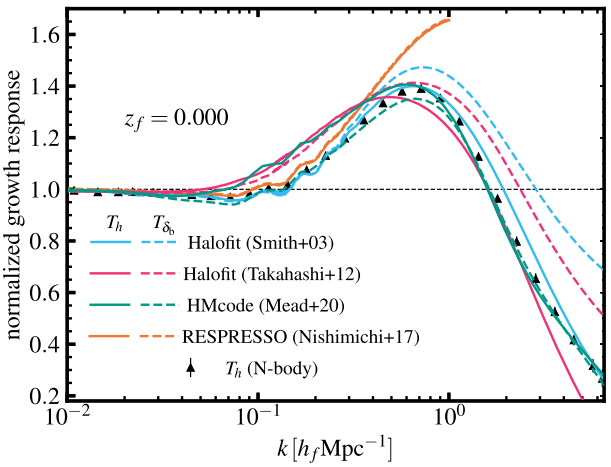

FIG. 3. Comparison of the simulation results of T_h and T_{δ_b} at $z_f = 0$ with the predictions computed from the public codes of nonlinear matter power spectrum: "Smith + 03 `Halofit`" [20], "Takahashi + 12 `Halofit`" [23], "Mead + 20 `HMcode`" [28], and "Nishimichi + 17 `RESPRESSO`" [72]. Here we used the public codes to compute the normalized responses from numerical derivative of the power spectrum predictions with models varying Ω_K or h (see text for details). The solid and dashed lines show the model predictions for T_h and T_{δ_b}, respectively. The triangle symbols are the same as in Fig. 2. We omit the simulation result for T_{δ_b} as it is very close to the triangle symbols, to avoid crowdedness in the figure.

$T_{\delta_b}(k)$ from Eq. (13) based on the SU method; we compute $\tilde{P}(k,z)$ for varied Ω_K-ΛCDM models assuming that the fitting formula is valid for nonflat cosmologies, respectively, and then compute $T_{\delta_b}(k)$ from numerical derivative. Here we adopt $\delta_b = \pm 0.01$ at $z_f = 0$. On the other hand, for $T_h(k)$, we vary only h with keeping the linear matter power spectrum fixed (keeping $\Omega_m h^2$ fixed as discussed around Table I) in flat models, and then compute $T_h(k)$ from numerical derivative of the fitting formula predictions, where we adopt variations of $\delta h = \pm 0.02$. The figure shows that none of the fitting formulas reproduces the approximate identity of $T_{\delta_b} \approx T_h$ in nonlinear regime at the level that we see in the responses measured from N-body simulations [also see Ref. [27], for the similar discussion]. This implies that the fitting formulas have a degraded accuracy for nonflat cosmologies in the nonlinear regime, because the response to δ_b is equivalent to the dependence of $P(k)$ on Ω_K. Nevertheless it is intriguing to find that Smith + 03 and Takahashi + 12 `Halofit` give a closer prediction to the simulation result for the response to h, than that to δ_b. In particular, the result for Smith + 03 `Halofit` appears to be promising, including a better agreement over the transition scales between the linear and nonlinear regimes.

In Fig. 3, we also show the response computed using `RESPRESSO` [72]. It reconstructs the nonlinear power spectrum from an input linear power spectrum at a target redshift for a target cosmological model based on the perturbation theory motivated method starting from a nonlinear matter power spectrum at a fiducial cosmology measured from N-body simulations at a different redshift. The output redshift of the nonlinear matter power spectrum

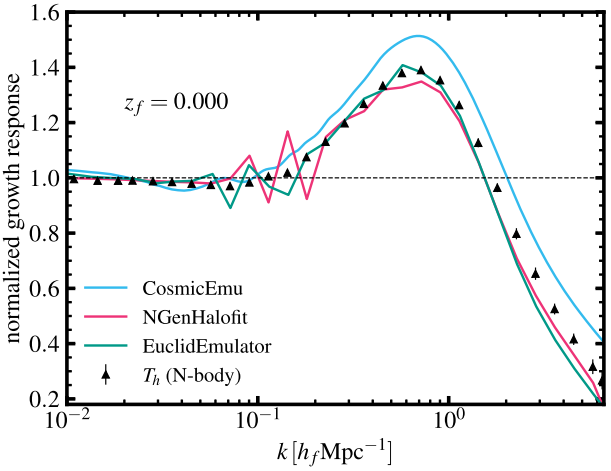

FIG. 4. Similar to the previous figure, but this figure compares the simulation result for T_h at $z_f = 0$ with those computed from the public emulator of the nonlinear matter power spectrum: `CosmicEmu` [24], `NGenHalofit` [29] and `EuclidEmulator` [30]. These emulators are designed to compute the power spectrum for flat-geometry CDM cosmologies, so here we compare the results for T_h.

at a fiducial cosmology is chosen to minimize the difference of the linear power spectra for target and fiducial cosmologies. The difference in the nonlinear power spectra in k bin between the two cosmologies is computed by summing up the contributions from the band power of the linear power spectrum in each q bin. To do this, the diagrams in the perturbative expansion relevant to the response of the nonlinear power spectrum to the linear counterpart are precomputed at different values of $\Omega_{\rm m}$, and this lookup table is inferred along a path between the fiducial and the target cosmology. However, since the fiducial cosmology adopted in RESPRESSO is identical to ours and all cosmologies considered in this paper share the same shape of the linear power spectrum, the difference in the linear power spectrum in q bin between the two cosmologies vanishes. In this case, the difference in the nonlinear power spectra in k bin between the two cosmologies vanishes and the estimated response can only be sourced by the time evolution of the nonlinear power spectrum for the fiducial cosmology. Hence, Fig. 3 clearly shows that the response to the redshift fails to reproduce the response to h (or $\delta_{\rm b}$) in the nonlinear regime. Note that RESPRESSO outputs the predictions up to $k \sim 1\ h{\rm Mpc}^{-1}$. Since RESPRESSO needs only the linear power spectrum of the target cosmology as input, its prediction is unique for models with the same linear power spectrum (e.g., two models with different values of $A_{\rm s}$, but evaluated at different redshifts to match the normalization of the linear power spectrum), even when the growth history is different. Hence T_h and $T_{\delta_{\rm b}}$ computed by RESPRESSO are indistinguishable except for the slight difference due to numerical accuracy. However, since RESPRESSO is motivated by

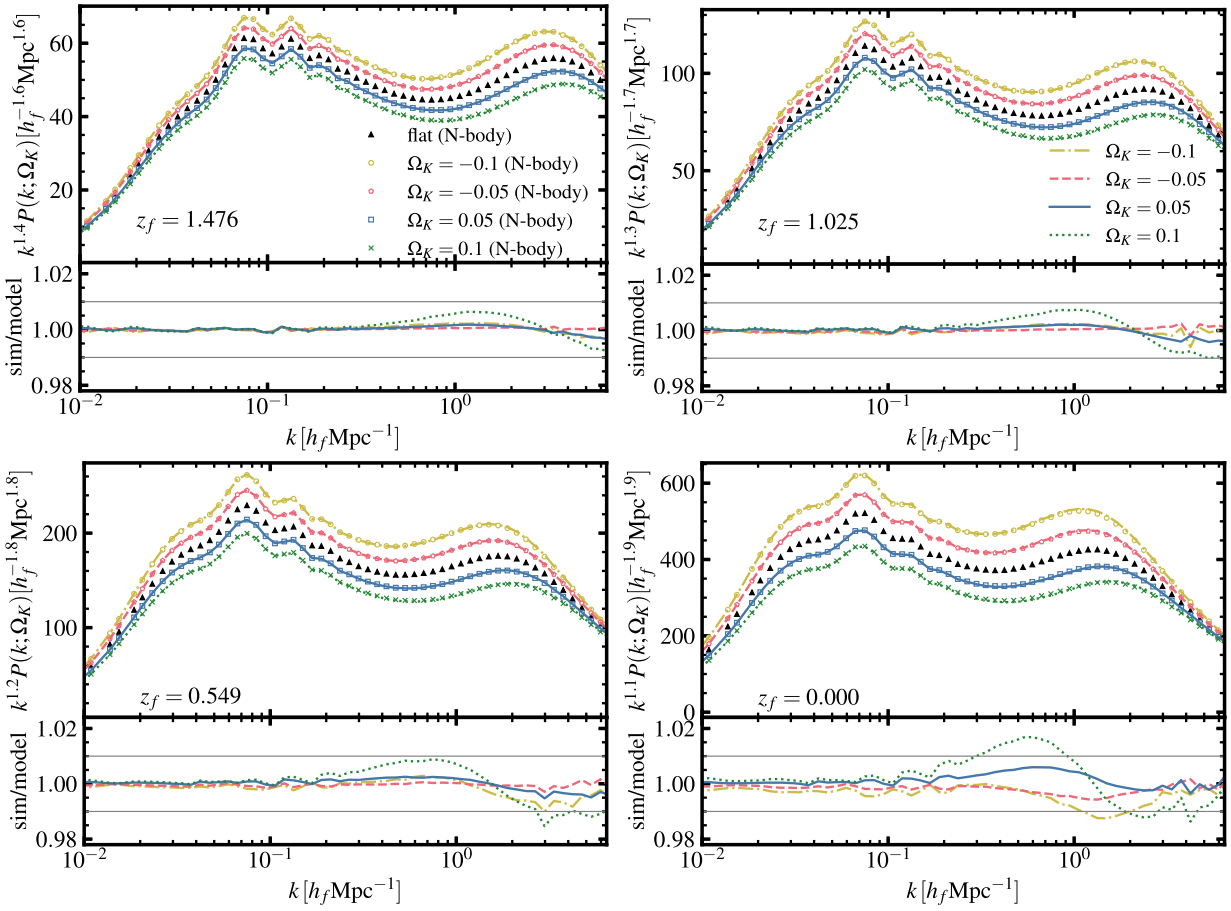

FIG. 5. An assessment of the accuracy of our method (Eq. (18) for predicting $P(k)$ for nonflat ΛCDM models. The different symbols in each panel denote $P(k)$, directly estimated from N-body simulations for nonflat models with $\Omega_K = \pm 0.05$ and ± 0.1 (Ω_K-ΛCDM2 and Ω_K-ΛCDM3 models in Table I), at each of the four redshifts, while the lines denote the results from our method, $\tilde{P}(k)$ in Eq. (18). Note that we used the simulation results for $P_f(k, z_f)$ and $T_h(k, z_f)$ in Eq. (18). For the simulation results we used the "paired-and-fixed" method in Angulo and Pontzen [61] to reduce the stochasticity. For comparison we also show the simulation result for the flat fiducial simulation by triangle symbols. For illustrative purpose we show $k^\alpha P(k, z)$ where the power index α for each redshift output is chosen in that the y-range is narrower in the linear scale. The lower plot in each panel shows the ratio between the simulation result and our method. The horizontal lines denote $\pm 1\%$ fractional accuracy.

the perturbation theory, these predictions begin to differ from the responses measured from N-body simulations around $k \sim 0.2\ h\mathrm{Mpc}^{-1}$, which corresponds to the scale where the perturbation theory fails. This is similar to the results from Ref. [53] (see Fig. 2 in the paper), where the perturbation theory (1-loop) predictions were used to compute the response up to quasi nonlinear regime. These results indicate that the perturbation theory motivated model fails to predict the responses in the nonlinear regime. That is, as we discussed above, the nonlinear power spectrum has other dependencies besides the linear power spectrum (also see Appendix for the similar discussion).

In Fig. 4 we use the publicly-available emulators of $P(k)$, built for flat cosmologies, to assess accuracy for predicting the response to h. Here we used `CosmicEmu` [24], `NGenHalofit` [29], and `EuclidEmulator` [30]. The later two emulators fairly well reproduce the simulation results, although a jagged feature in the numerical derivative is seen, probably due to a k-binning issue (or interpolation issue) in the output.

B. Accuracy of the approximation of $P(k)$ for nonflat ΛCDM

In this section we assess an accuracy of the approximation [Eq. (18)] to evaluate $P(k)$ for Ω_K-ΛCDM model, by comparing the predictions based on the method with the power spectra directly measured from N-body simulations for Ω_K-ΛCDM model.

The data points in Fig. 5 show $P(k)$ estimated from the simulations, in Table I, for Ω_K-ΛCDM models with $\Omega_K = \pm\{0.05, 0.1\}$, at each of the four redshifts. The curves in each panel show the predictions computed based on Eq. (18), where we used the normalized response T_h, computed from the simulations (the results in Fig. 2), and the power spectrum $P_f(k, z_f)$ computed from the fΛCDM simulation (the triangle symbols). The figure shows that the estimator reproduces the simulation result at an accuracy better than ∼1% in the amplitude over the wide range of wave numbers, except for ∼2% accuracy for $\Omega_K = 0.1$ at $k \sim 1\ h_f\mathrm{Mpc}^{-1}$ that corresponds to the largest δ_b. The 1%

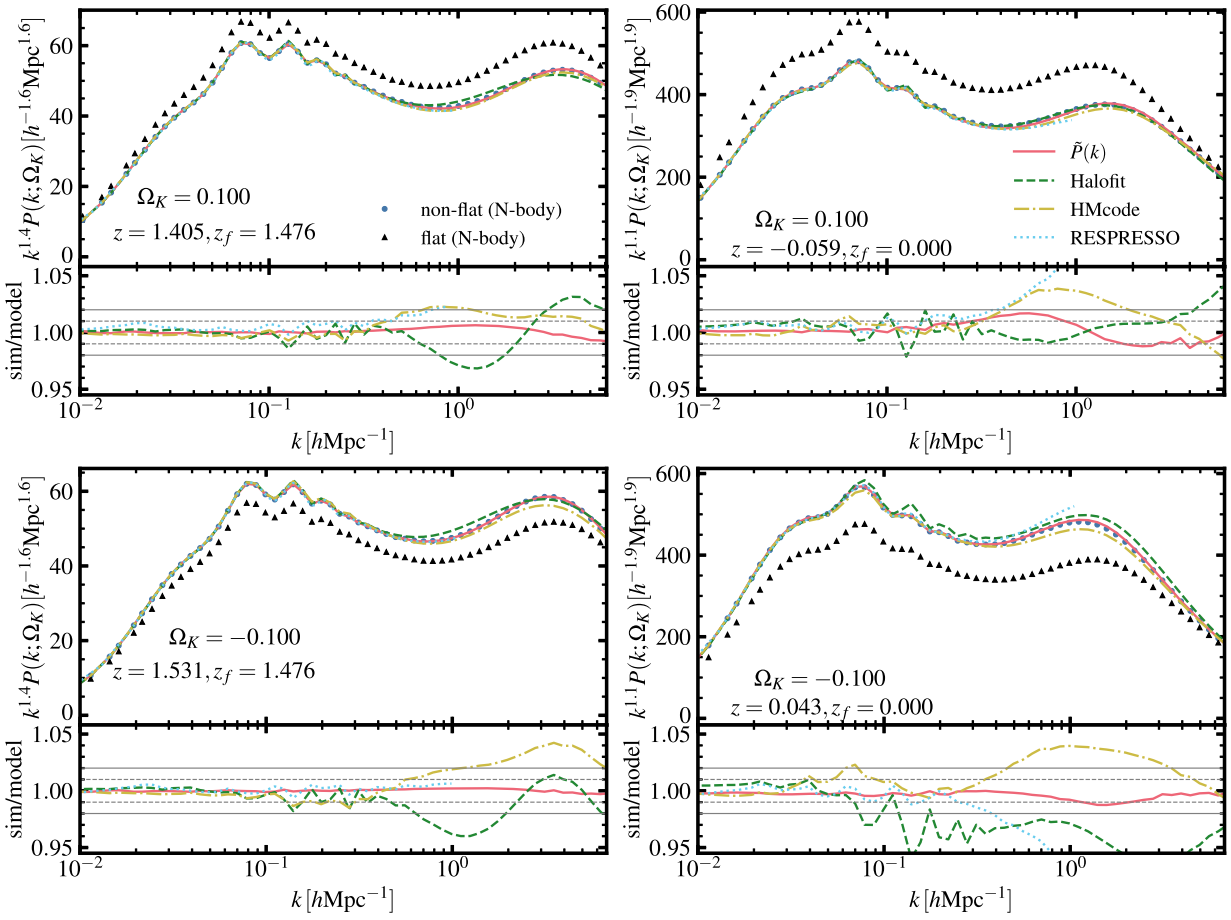

FIG. 6. Similar to the previous figure, but this figure compares the nonlinear matter power spectra that are computed from our method and the public codes, for the Ω_K-ΛCDM3 model with $\Omega_K = \pm 0.1$. Here we consider `Halofit` [23], `HMcode` [28] and `RESPRESSO` [72]. The solid line in each panel is the same as in the previous figure, while the other lines denote the results computed from the codes, where we used the direct predictions for nonflat models. The horizontal dashed and solid lines denote ±1% and ±2% fractional accuracy, respectively.

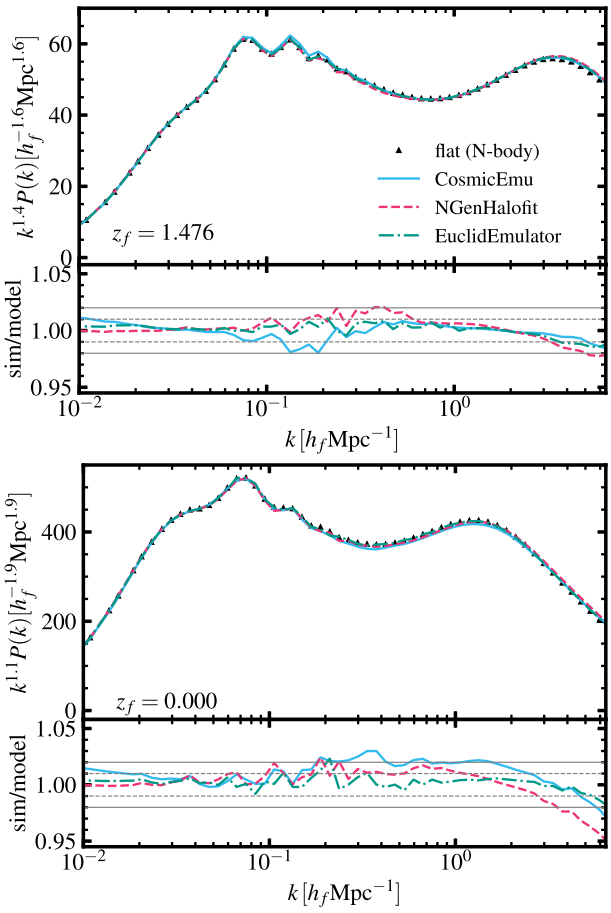

FIG. 7. Comparison of nonlinear power spectra for flat cosmology at $z_f = 1.476$ (top) $z_f = 0$ (bottom) computed from our simulations and the public emulators. Here we consider `CosmicEmu` [25], `NGenHalofit` [29], and `EuclidEmulator` [30]. The horizontal dashed and solid lines denote $\pm 1\%$ and $\pm 2\%$ fractional accuracy, respectively.

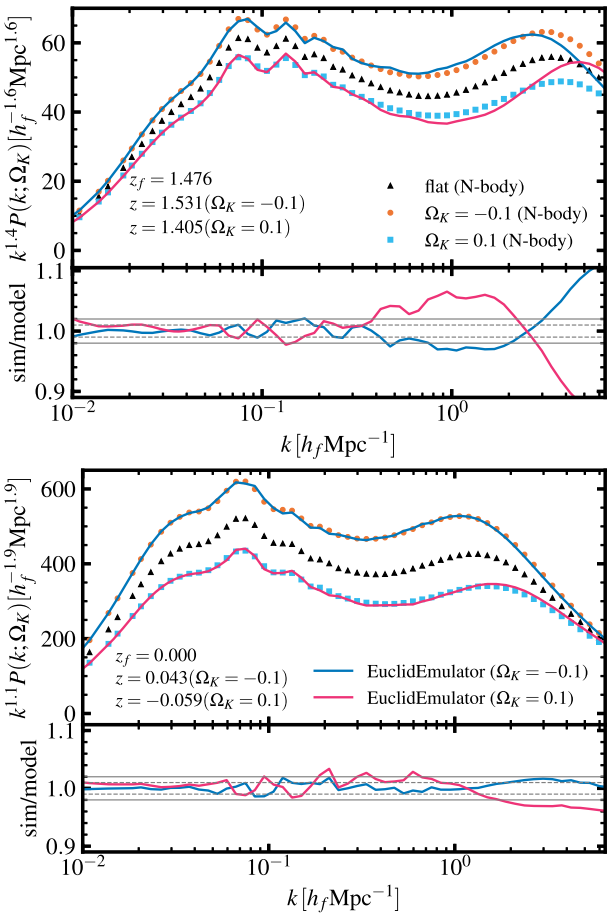

FIG. 8. Performance of our method [Eq. (17)] for predicting the nonlinear matter power spectrum for nonflat ΛCDM model with $\Omega_K = \pm 0.1$, at $z_f = 1.476$ (top) and $z_f = 0$ (bottom). Here we use `EuclidEmulator` [30] predictions for $P_f(k, z_f)$ and $T_h(k, z_f)$ in Eq. (18). The horizontal dashed and solid lines denote $\pm 1\%$ and $\pm 2\%$ fractional accuracy, respectively.

accuracy at $k \sim 1\ h_f^{-1}$ Mpc roughly meets requirements on $P(k)$ for upcoming weak lensing surveys [39].

In Fig. 6, we compare the performance of the estimator predictions [Eq. (18)] with public codes for each cosmological model. Here we consider two fitting formulas, `Halofit` in Takahashi *et al.* [23] and `HMcode` [28]. In addition, we consider `RESPRESSO` [72]. Although these models are calibrated under $\Omega_K = 0$, we use their direct predictions for nonflat cosmologies using an extrapolation to $\Omega_K \neq 0$. While the accuracy of `Halofit`, `HMcode` and `RESPRESSO` vary with the redshift, the estimator prediction displays a better performance than the public codes especially in the nonlinear regime.

Now we study the accuracy of the emulators of $P(k)$, calibrated only for flat cosmologies, to predict $P(k)$ for nonflat models, based on our method [Eq. (18)]. Before going to the result, in Fig. 7, we assess the performance of the emulators by comparing the predictions with the simulation results for the fiducial flat model. All the emulators reproduce the simulation results to within $\sim 2\%$ up to $k \sim 1\ h_f\mathrm{Mpc}^{-1}$.

In Fig. 8 we apply our method to the `EuclidEmulator` for predicting $P(k)$ for the nonflat models with $\Omega_K = \pm 0.1$, compared to the simulation results, where we use the emulator to compute $T_h(k, z_f)$ and $P_f(k, z_f)$ and then plug those into Eq. (18) to obtain $\tilde{P}(k, z)$ for the target Ω_K-ΛCDM model. The predictions by `EuclidEmulator` are in good agreement with the simulations at $z_f = 0$ to within $\sim 2\%$ even for the relatively large $|\Omega_K|$ models, while the accuracy is degraded especially at high-k for $z_f \simeq 1.5$. The nice agreement for $z_f = 0$ is encouraging, and the accuracy of the emulator for the high redshift might need to be further studied.

V. DISCUSSION AND CONCLUSION

In this paper we have developed an approximate method to compute the nonlinear matter power spectrum, $P(k)$, for

a "nonflat" ΛCDM model, from quantities computed for the counterpart flat ΛCDM model, based on the separate universe (SU) method. To do this, we need to employ a specific mapping of the cosmological parameters and redshifts between the nonflat and flat models, with keeping the initial power spectrum fixed. In addition we utilized the fact that the normalized response of $P(k)$ to the long-wavelength fluctuation mode $\delta_{\rm b}$ in the flat model is well approximated by the normalized response to h for the flat model, which was validated by using the N-body simulations. We showed that our method [Eq. (18)] enables to compute $P(k)$ for nonflat models with $|\Omega_K| \leq 0.1$, to the fractional accuracy of $\sim 1\%$ compared to the N-body simulation results, over the range of scales up $k \lesssim 6\ h{\rm Mpc}^{-1}$ and in the range $0 \leq z \lesssim 1.5$, *if* the accurate response function is available. Encouragingly, even if we use the publicly available emulator of $P(k)$, which is calibrated for flat cosmologies (e.g., `EuclidEmulator` [30]), our method allows one to compute $P(k)$ for nonflat model, to within the accuracy of $\sim 2\%$.

A key ingredient in our approach is that how the derivative operation with respect to Ω_K should be performed exactly in a multidimensional input parameter space under a constraint, $\Omega_K = 1 - (\Omega_{\rm m} + \Omega_\Lambda)$. In our case, the SU approach guides us to use $\delta_{\rm b}$ to fully specify the direction along which the derivative is taken. Then, we numerically find that this derivative coincides well with the derivative with respect to h within flat cosmologies. This turns out to be practically useful to model nonflat cosmologies using only the knowledge within flat cosmologies. We can consider different ways to match flat-ΛCDM and Ω_K-ΛCDM models, or more general models such as wCDM models with the equation-of-state parameter w for dark energy. It might be of interest to study more about the similarities and differences of the responses with respect to different combinations of parameters, as well as the time variable, at the nonlinear level beyond the applicable range of the one-to-one correspondence between $P(k)$ and $P^{\rm L}(k)$, which is valid within the EdS approximation and is explicitly used in methods such as `RESPRESSO`. We will postpone to address a more comprehensive study in this direction as a future work.

An obvious application is to apply the method to actual data for constraining the curvature parameter Ω_K. We will explore this direction in our future work. It is really interesting to explore a constraint of Ω_K from galaxy surveys, independently from the CMB constraint. As discussed in Ref. [9], if we have precise BAO measurements at multiple redshifts (more than 3 redshifts), we can constrain Ω_K without employing any prior on the sound horizon (BAO scale) from CMB, because such multi-redshift BAO measurements can give sufficient information on the sound horizon scale and the cosmological distances that depend on $\Omega_{\rm m}$ and Ω_K (Ω_Λ is set by the identity $\Omega_K = 1 - [\Omega_{\rm m} + \Omega_\Lambda]$) for nonflat ΛCDM models. However, note that the galaxy BAO geometrical constraints need to assume the existence of the standard ruler (i.e., BAO scale) over the multiple redshifts, as supported by the adiabatic initial condition, and the constraints would be degraded if employing further extended models such as time-varying dark energy models. In addition, we should try to explore the curvature information from the growth history of cosmic structures, in addition to the geometrical constraints. Once such high-precision constraint on Ω_K is obtained from galaxy surveys, we can address whether the *Planck* constraint and galaxy surveys, or more generally the late-time universe, are consistent with each other within the adiabatic ΛCDM framework. Any deviation or inconsistency in these tests would be a smoking gun evidence of new physics beyond the standard ΛCDM model, and this will be definitely an interesting and important direction to explore with actual datasets.

The response $T_{\delta_{\rm b}}$ is also a key quantity for calibrating the super sample covariance (SSC), which is a dominant source of the non-Gaussian errors in the correlation functions of cosmic shear [41,73–75]. For future weak lensing surveys, it is important to obtain an accurate calibration of the non-Gaussian covariance, e.g., to have a proper assessment of the best-fit model compared with the statistical errors and not to have any significant bias in estimated parameters in the parameter inference [76]. Estimating the SSC term for an arbitrary cosmological model is computationally expensive, because it requires to run a sufficient number of SU simulations (including the simulations in nonflat cosmologies) to have an accurate estimation of the SSC terms. For this, the approximation of $T_{\delta_{\rm b}} \approx T_h$ is also useful because we can use the public code of $P(k)$ to compute the SSC for a given cosmological model. However, note that, to model the total power of the SSC term, we further need to take into account the dilation effect [42], which is straightforward to compute from the numerical derivative of the nonlinear power spectra with respect to k.

The SSC term is also significant or not negligible for galaxy-galaxy weak lensing or galaxy clustering, respectively [77]. The SSC terms for these correlation functions arise from the responses of the matter-galaxy or galaxy-galaxy power spectra, $P_{\rm gm}$ or $P_{\rm gg}$, to the super survey mode, $\delta_{\rm b}$. Since the galaxy-halo connection is modeled by the halo occupation distribution (HOD) model, it is interesting to study whether the normalized growth response of the matter-galaxy (matter-halo) or galaxy-galaxy (halo-halo) power spectra to $\delta_{\rm b}$ is approximated by the normalized response to h similarly to the case for the matter power spectrum. This is our future work and will be presented elsewhere.

ACKNOWLEDGMENTS

We would like to thank Kaz Akitsu, Takahiko Matsubara, Ravi Sheth, and Masato Shirasaki for their useful and stimulating discussion. We thank the Yukawa Institute for Theoretical Physics at Kyoto University for

their warm hospitality, where this work was partly done during the YITP-T-21-06 workshop on "Galaxy shape statistics and cosmology". This work was supported in part by World Premier International Research Center Initiative (WPI Initiative), MEXT, Japan, JSPS KAKENHI Grants No. JP22H00130, No. JP20H05850, No. JP20H05855, No. JP20H05861, No. JP20H04723, No. JP19H00677, No. JP21H01081, No. JP22K03634, Basic Research Grant (Super AI) of Institute for AI and Beyond of the University of Tokyo, and Japan Science and Technology Agency (JST) AIP Acceleration Research Grant No. JP20317829. Numerical computations were carried out on Cray XC50 at Center for Computational Astrophysics, National Astronomical Observatory of Japan.

APPENDIX: VALIDATION OF THE POWER SPECTRUM RESPONSES WITH HALO MODEL

In this section we study whether the approximate identity of $T_{\delta_b}(k) \approx T_h(k)$ is reproduced by the halo model [78].

1. Halo model approach

The halo model gives a useful (semi-)analytical description of the nonlinear clustering statistics, and allows us to study the power spectrum responses [see [41,42,79], for the similar study]. In the halo model, the power spectrum is given by sum of the 1- and 2-halo terms as

$$P(k) = P^{1h}(k) + P^{2h}(k), \tag{A1}$$

where

$$P^{1h}(k) \equiv \int \mathrm{d}M n(M) \left(\frac{M}{\bar{\rho}_m}\right)^2 \tilde{u}_M(k)^2 \tag{A2}$$

and

$$P^{2h}(k) \equiv [I_1^1(k)]^2 P^L(k). \tag{A3}$$

with the function defined as

$$I_\mu^\beta(k_1, \ldots, k_\mu) \equiv \int \mathrm{d}M n(M) \left(\frac{M}{\bar{\rho}_m}\right)^\mu b_\beta(M) \prod_{i=1}^{\mu} \tilde{u}_M(k_i), \tag{A4}$$

where $n(M)\mathrm{d}M$ is the number density of halos in the mass range $[M, M + \mathrm{d}M]$ (i.e., the halo mass function), $b_\beta(M)$ is the bias parameter for halos with mass M, defined in that $b_0 = 1$ and $b_1(M)$ is the linear bias parameter, and $\tilde{u}_M(k)$ is the Fourier transform of the mass density profile of halos with mass M. Note that the halo profile is normalized so as to satisfy $\tilde{u}_M(k) \to 1$ at $k \to 0$. With this normalization, $I_1^1(k)$ should be normalized at very small k so as to satisfy the linear limit $I_1^1(k) \to 1$ at $k \to 0$ in that the 2-halo term reproduces the linear matter power spectrum, $P^{2h}(k) \simeq P^L(k)$. For the halo mass density profile, we assume the Navarro-Frenk-White (NFW) halo profile [80] in the following, where we estimate the halo concentration for halos in each mass bin from simulations.

We can formally express the power spectrum response with respect to a parameter p ($p = \delta_b$ or h) as

$$\frac{\partial P(k)}{\partial p} = \frac{\partial P^{1h}(k)}{\partial p} + \frac{\partial P^{2h}(k)}{\partial p} \tag{A5}$$

where the 1-halo term response is given as

$$\frac{\partial P^{1h}(k)}{\partial p} = \int \mathrm{d}M n(M) \left(\frac{M}{\bar{\rho}_m}\right)^2 \tilde{u}_M(k)^2 \times \left[\frac{\partial \ln n(M)}{\partial p} + 2\frac{\partial \ln \tilde{u}_M(k)}{\partial p}\right]. \tag{A6}$$

The 2-halo term response is given as

$$\frac{\partial P^{2h}(k)}{\partial p} = 2I_1^1(k)\frac{\partial I_1^1(k)}{\partial p} P^L(k) + [I_1^1(k)]^2 \frac{\partial P^L(k)}{\partial p}. \tag{A7}$$

Here the 2nd term, i.e., the linear power spectrum response $\partial P^L/\partial p$, is equivalent to the response of the linear growth factor as discussed in Sec. II C. Hence it is straightforward to compute the 2nd term using the linear growth factor. Since the 2-halo term gives a dominant contribution to the total power in the linear regime, where $I_1^1 \simeq 1$ as discussed above, we ignore the 1st term for the following results, for simplicity.

2. Evaluation with N-body simulation

In this section we use the N-body simulations in Table I to calibrate each term of the 1-halo term response [Eq. (A6)]; more exactly, the responses of the halo mass function and the halo mass density profile.

First we need to define halos from each output of N-body simulations. We follow the method in Nishimichi *et al.* [26], so please see the paper for further details. As we emphasize around Table I, all the N-body simulations employ the same box size ($L \simeq 1.49$ Gpc), the same N-body particle number (2048^3) and the same N-body mass scale ($m_p = 1.52 \times 10^{10}\ M_\odot$). In this setting, the mean comoving mass density $\bar{\rho}_{m0}$ is the same for all the simulations. To identify halos in each simulation output, we use the public software `Rockstar` [81] that identifies halos and subhalos based on the clustering of N-body particles in phase space. For each halo/subhalo, we compute the spherical overdensity, $\Delta = 200$, to define mass of each halo/subhalo in the comoving coordinates, $M = (4\pi/3)(R_{200m})^3 \bar{\rho}_{m0} \Delta$. Note that the halo mass definition is different from that used in the study of halo bias

calibration using the SU simulations [e.g., [46]], where the spherical overdensity is set to be $\Delta = 200/(1+\delta_{\rm b})$ in the SU simulation so that halos are identified using the same *physical* overdensity as the corresponding global universe. By using this halo definition, we can estimate only the "growth" response for the 1-halo term, in the decomposition of "growth" and "dilation" responses [42]. Hence this response calibration is different from the method in [46].

After we identified halo candidates, we determine whether they are central or satellite halos. When the separation of two different halos (between their centers) is closer than $R_{\rm 200m}$ of the more massive one, we mark the less massive one as a satellite halo. In the following we use only central halos with mass containing more than 100 particles. With these definitions, each halo in all the simulations contains exactly the same number of member particles, which allows a cleaner calibration of the power spectrum responses in the halo model approach.

We first estimate the halo mass function from the halo catalog in each simulation realization. We use the following fitting function, which is a modified version of the earlier work in Press and Schechter [also see [82,83]], to fit the mass function estimated from the simulation:

$$n(M) \equiv \frac{{\rm d}n}{{\rm d}M} = f(\sigma_M)\frac{\bar{\rho}_{\rm m0}}{M}\frac{{\rm d}\ln\sigma_M^{-1}}{{\rm d}M}, \tag{A8}$$

with

$$f(\sigma_M) = A\left[\left(\frac{\sigma_M}{b}\right)^a + 1\right]\exp\left(-\frac{c}{\sigma_M^2}\right), \tag{A9}$$

where A, a, b, and c are fitting parameters. The mass variance σ_M^2 is defined as

$$\sigma_M(z)^2 \equiv \int \frac{k^2{\rm d}k}{2\pi^2}P^{\rm L}(k,z)|\tilde{W}_R(k)|^2, \tag{A10}$$

where $\tilde{W}_R(k)$ is the Fourier transform of a top-hat filter of radius R that is specified by an input halo mass via $R = (3M/4\pi\bar{\rho}_{\rm m0})^{1/3}$.

For each of the simulations for Ω_K-ΛCDM1 and h-ΛCDM models in Table I, we estimate the best-fit values of A and a by fitting the above formula to the mass function measured from each simulation, assuming the Poisson noise in each halo mass bin. For the parameters b and c, we fixed their values to those in Tinker *et al.* [84]. We use 10 realizations for each of the models with $\delta_{\rm b} = \pm 0.01$ at $z_f = 0$ (Ω_K-ΛCDM1) and the positive or negative variations of h from its fiducial value (h-ΛCDM). We then estimate the responses of the halo mass function with respect to $\delta_{\rm b}$ or h from the averaged mass function, using the two-side numerical derivatives: $\partial\ln n(M)/\partial\delta_{\rm b}$ or $\partial\ln n(M)/\partial h$, which is the first term of the 1-halo term response [Eq. (A6)]. Note that this corresponds to the growth response of halo mass function due to the reason we described above. Figure 9 shows the results for the mass function responses at $z_f = 0$. Here we normalized the responses in the same way as those in $T_{\delta_{\rm b}}$ and T_h using the responses of the linear growth factor [see around Eq. (13)]. The figure shows that the responses are in remarkably nice agreement with each other. This agreement supports that the halo mass function is approximately given by a "universal" form, i.e., $f(\nu)$, where $\nu \equiv \delta_{\rm c}/\sigma_M(z)$ ($\delta_{\rm c}$ is a critical collapse threshold) or $\nu \propto 1/\sigma_M(z)$, for different cosmological models. In this case, the halo mass function response is given by $\partial\ln n(M)/\partial p \propto \partial\ln f/\partial\nu \times \partial\nu/\partial p = -\partial\ln f/\partial\ln\nu \times \partial\ln D/\partial p$, since $\sigma_M(z) \propto D(z)$. Note that we estimated the parameters A and a independently for different cosmological models, so the universality breaks down if the parameters A and a differ in the different models.

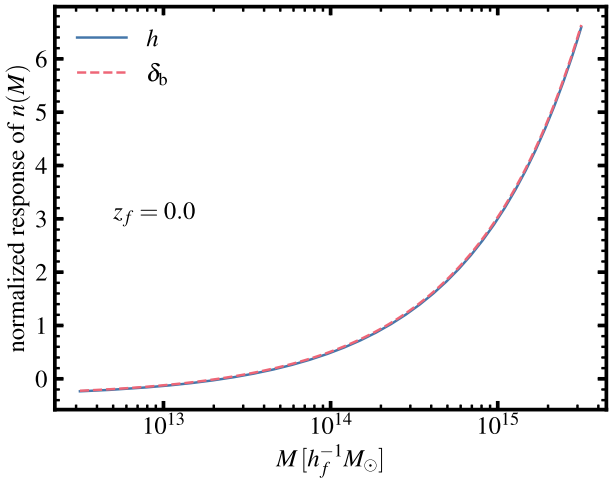

FIG. 9. Normalized response of the halo mass function, $n(M)$, to $\delta_{\rm b}$ or h at $z_f = 0$, where the normalization was done in the same was as in Fig. 2. These are computed from the halo catalogs in the N-body simulations for Ω_K-ΛCDM1 and h-ΛCDM models in Table I (see test for details). The two responses are in good agreement with each other.

Next we employ the following method to estimate the responses of the halo mass density profile, which is the 2nd term of Eq. (A6), in each simulation. We divide halos into each of 20 logarithmically-spaced mass bins in the range of $M = [10^{12.45}, 10^{15.45}]\ h_f^{-1}M_\odot$, and measure the "averaged" halo mass profile of halos in each bin. We fit each of the estimated mass profiles by an NFW profile to estimate the best-fit concentration parameter, assuming the Poisson errors according to the number of N-body particles contained in each of the radial bins. We then compare the best-fit NFW profiles to estimate the responses of the halo mass concentration with respect to the variations of $\delta_{\rm b} = \pm 0.01$ at $z_f = 0$ and $\delta h = \pm 0.02$, from the simulations for Ω_K-ΛCDM1 and h-ΛCDM models. Figure 10 shows the

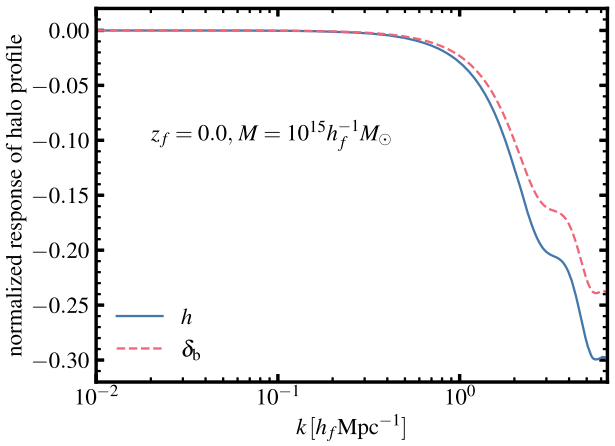

FIG. 10. Normalized response of the Fourier transform of the halo mass density profile, $\tilde{u}_M(k)$, to δ_b or h for halos in the mass bin of $M = 10^{15}\ h_f^{-1} M_\odot$ at $z_f = 0$, as in the previous figure. To compute this, we first fit the averaged mass profile of halos in the mass bin by an NFW profile to obtain the halo concentration in the simulations for each of the Ω_K-ΛCDM1 and h-ΛCDM model with varying δ_b or h. Then we estimated the variations in the halo mass concentration between the varied cosmological models. The figure shows the results where we insert the variations of the halo mass concentration into the NFW profile (see text for details).

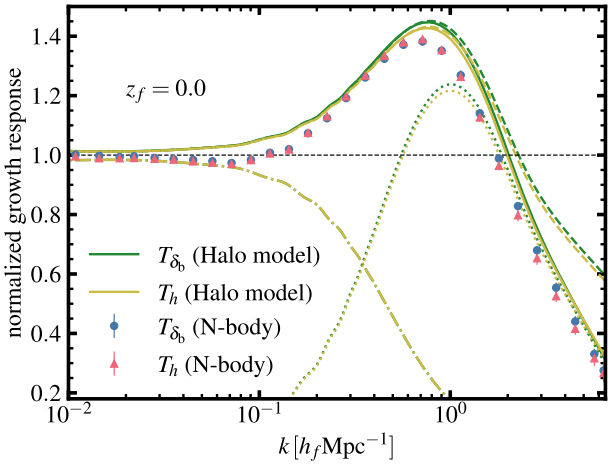

FIG. 11. Solid lines show the halo model predictions for the normalized responses of matter power spectrum to δ_b and h, i.e., T_{δ_b} and T_h, at $z_f = 0$. The dotted and dot-dashed lines show the 1- and 2-halo term predictions, respectively. The dashed lines denote the halo model predictions where we ignored the responses of the halo mass density profile or equivalently when we include only the halo mass function responses. For comparison, we show the simulation results for T_{δ_b} and T_h which are the same as those in the lower-right panel of Fig. 2.

responses of $\tilde{u}_M(k)$ with respect to δ_b and h for halos with $10^{15} h_f^{-1}\ M_\odot$ at $z_f = 0$, where we employ the same normalization as in Fig. 9. To estimate these responses, we plug in the variations of the halo concentration parameters into the Fourier transform of NFW profile. Note that the responses are by definition vanishing in small k bins, where the normalized profile $u_M(k) = 1$. The figure shows that the halo profile responses show a sizable difference at scales, where $u_M(k) < 1$. The difference implies that the two responses do not exactly agree with each other at large k in the nonlinear regime. This difference would be the origin of the slight discrepancy in T_{δ_b} and T_h at $k \gtrsim 1\ h_f\mathrm{Mpc}^{-1}$.

Figure 11 shows the normalized growth responses of matter power spectrum with respect to δ_b and h, $T_{\delta_b}(k)$ and $T_h(k)$, which are computed using the halo model: the sum of the 1-halo and 2-halo terms [Eqs. (A6) and (A7)]. To compute these results, we used the results of Figs. 9 and 10. First, the figure clearly shows that the halo model predictions for T_{δ_b} and T_h agree well with each other. As expected, the scale-dependent responses arise from the 1-halo term, and the responses at $k \gtrsim 1\ h_f\mathrm{Mpc}^{-1}$ arises from the responses of the halo mass density profile. Thus these results give another confirmation of the approximate consistency of T_{δ_b} and T_h for ΛCDM model. However, the halo model cannot well reproduce the simulation results for the power spectrum response, especially at transition scales between the 1- and 2-halo terms, reflecting the limitation of the halo model.

[1] S. Weinberg, *Gravitation and Cosmology: Principles and Applications of the General Theory of Relativity* (Wiley-VCH, Weinheim, Germany, 1972).
[2] K. Sato, Mon. Not. R. Astron. Soc. **195**, 467 (1981).
[3] A. H. Guth, Phys. Rev. D **23**, 347 (1981).
[4] S. Coleman and F. De Luccia, Phys. Rev. D **21**, 3305 (1980).
[5] J. R. Gott, Nature (London) **295**, 304 (1982).
[6] A. H. Guth and Y. Nomura, Phys. Rev. D **86**, 023534 (2012).
[7] M. Kleban and M. Schillo, J. Cosmol. Astropart. Phys. 06 (2012) 029.
[8] M. Takada, R. S. Ellis, M. Chiba, J. E. Greene, H. Aihara, N. Arimoto, K. Bundy, J. Cohen, O. Doré, G. Graves *et al.*, Publ. Astron. Soc. Jpn. **66**, R1 (2014).
[9] M. Takada and O. Doré, Phys. Rev. D **92**, 123518 (2015).
[10] G. Jungman, M. Kamionkowski, A. Kosowsky, and D. N. Spergel, Phys. Rev. D **54**, 1332 (1996).
[11] D. J. Eisenstein, I. Zehavi, D. W. Hogg, R. Scoccimarro, M. R. Blanton, R. C. Nichol, R. Scranton, H.-J. Seo, M. Tegmark, Z. Zheng *et al.*, Astrophys. J. **633**, 560 (2005).
[12] P. J. E. Peebles and J. T. Yu, Astrophys. J. **162**, 815 (1970).

[13] R. A. Sunyaev and Y. B. Zeldovich, Astrophys. J. Suppl. Ser. **7**, 3 (1970).
[14] N. A. Bahcall, J. P. Ostriker, S. Perlmutter, and P. J. Steinhardt, Science **284**, 1481 (1999).
[15] Planck Collaboration, N. Aghanim, Y. Akrami, M. Ashdown, J. Aumont, C. Baccigalupi, M. Ballardini, A. J. Banday, R. B. Barreiro, N. Bartolo *et al.*, Astron. Astrophys. **641**, A6 (2020).
[16] S. Alam, M. Aubert, S. Avila, C. Balland, J. E. Bautista, M. A. Bershady, D. Bizyaev, M. R. Blanton, A. S. Bolton, J. Bovy *et al.*, Phys. Rev. D **103**, 083533 (2021).
[17] E. Abdalla, G. F. Abellán, A. Aboubrahim, A. Agnello, Ö. Akarsu, Y. Akrami, G. Alestas, D. Aloni, L. Amendola, L. A. Anchordoqui *et al.*, J. High Energy Astrophys. **34**, 49 (2022).
[18] T. Tröster, M. Asgari, C. Blake, M. Cataneo, C. Heymans, H. Hildebrandt, B. Joachimi, C.-A. Lin, A. G. Sánchez, A. H. Wright *et al.*, Astron. Astrophys. **649**, A88 (2021).
[19] J. A. Peacock and S. J. Dodds, Mon. Not. R. Astron. Soc. **280**, L19 (1996).
[20] R. E. Smith, J. A. Peacock, A. Jenkins, S. D. M. White, C. S. Frenk, F. R. Pearce, P. A. Thomas, G. Efstathiou, and H. M. P. Couchman, Mon. Not. R. Astron. Soc. **341**, 1311 (2003).
[21] K. Heitmann, M. White, C. Wagner, S. Habib, and D. Higdon, Astrophys. J. **715**, 104 (2010).
[22] K. Heitmann, D. Higdon, M. White, S. Habib, B. J. Williams, E. Lawrence, and C. Wagner, Astrophys. J. **705**, 156 (2009).
[23] R. Takahashi, M. Sato, T. Nishimichi, A. Taruya, and M. Oguri, Astrophys. J. **761**, 152 (2012).
[24] K. Heitmann, D. Bingham, E. Lawrence, S. Bergner, S. Habib, D. Higdon, A. Pope, R. Biswas, H. Finkel, N. Frontiere *et al.*, Astrophys. J. **820**, 108 (2016).
[25] E. Lawrence, K. Heitmann, J. Kwan, A. Upadhye, D. Bingham, S. Habib, D. Higdon, A. Pope, H. Finkel, and N. Frontiere, Astrophys. J. **847**, 50 (2017).
[26] T. Nishimichi, M. Takada, R. Takahashi, K. Osato, M. Shirasaki, T. Oogi, H. Miyatake, M. Oguri, R. Murata, Y. Kobayashi *et al.*, Astrophys. J. **884**, 29 (2019).
[27] P. Reimberg, F. Bernardeau, T. Nishimichi, and M. Rizzato, Mon. Not. R. Astron. Soc. **492**, 5226 (2020).
[28] A. J. Mead, S. Brieden, T. Tröster, and C. Heymans, Mon. Not. R. Astron. Soc. **502**, 1401 (2021).
[29] R. E. Smith and R. E. Angulo, Mon. Not. R. Astron. Soc. **486**, 1448 (2019).
[30] M. Knabenhans, J. Stadel, D. Potter, J. Dakin, S. Hannestad, T. Tram, S. Marelli, A. Schneider, R. Teyssier *et al.* (Euclid Collaboration), Mon. Not. R. Astron. Soc. **505**, 2840 (2021).
[31] W. Hu, Astrophys. J. Lett. **522**, L21 (1999).
[32] M. Takada and B. Jain, Mon. Not. R. Astron. Soc. **348**, 897 (2004).
[33] H. Hildebrandt, M. Viola, C. Heymans, S. Joudaki, K. Kuijken, C. Blake, T. Erben, B. Joachimi, D. Klaes, L. Miller *et al.*, Mon. Not. R. Astron. Soc. **465**, 1454 (2017).
[34] M. A. Troxel, N. MacCrann, J. Zuntz, T. F. Eifler, E. Krause, S. Dodelson, D. Gruen, J. Blazek, O. Friedrich, S. Samuroff *et al.*, Phys. Rev. D **98**, 043528 (2018).
[35] C. Hikage, M. Oguri, T. Hamana, S. More, R. Mandelbaum, M. Takada, F. Köhlinger, H. Miyatake, A. J. Nishizawa, H. Aihara *et al.*, Publ. Astron. Soc. Jpn. **71**, 43 (2019).
[36] T. Hamana, M. Shirasaki, S. Miyazaki, C. Hikage, M. Oguri, S. More, R. Armstrong, A. Leauthaud, R. Mandelbaum, H. Miyatake *et al.*, Publ. Astron. Soc. Jpn. **72**, 16 (2020).
[37] M. Asgari, C.-A. Lin, B. Joachimi, B. Giblin, C. Heymans, H. Hildebrandt, A. Kannawadi, B. Stölzner, T. Tröster, J. L. van den Busch *et al.*, Astron. Astrophys. **645**, A104 (2021).
[38] L. F. Secco, S. Samuroff, E. Krause, B. Jain, J. Blazek, M. Raveri, A. Campos, A. Amon, A. Chen, C. Doux *et al.*, Phys. Rev. D **105**, 023515 (2022).
[39] D. Huterer and M. Takada, Astropart. Phys. **23**, 369 (2005).
[40] T. Baldauf, U. Seljak, L. Senatore, and M. Zaldarriaga, J. Cosmol. Astropart. Phys. 10 (**2011**) 031.
[41] M. Takada and W. Hu, Phys. Rev. D **87**, 123504 (2013).
[42] Y. Li, W. Hu, and M. Takada, Phys. Rev. D **89**, 083519 (2014).
[43] Y. Li, W. Hu, and M. Takada, Phys. Rev. D **90**, 103530 (2014).
[44] C. Wagner, F. Schmidt, C. T. Chiang, and E. Komatsu, Mon. Not. R. Astron. Soc. **448**, L11 (2015).
[45] T. Lazeyras, C. Wagner, T. Baldauf, and F. Schmidt, J. Cosmol. Astropart. Phys. 02 (**2016**) 018.
[46] Y. Li, W. Hu, and M. Takada, Phys. Rev. D **93**, 063507 (2016).
[47] T. Baldauf, U. Seljak, L. Senatore, and M. Zaldarriaga, J. Cosmol. Astropart. Phys. 09 (**2016**) 007.
[48] A. E. Bayer, A. Banerjee, and U. Seljak, Phys. Rev. D **105**, 123510 (2022).
[49] W. Hu, C.-T. Chiang, Y. Li, and M. LoVerde, Phys. Rev. D **94**, 023002 (2016).
[50] K. Tomita, Prog. Theor. Phys. **37**, 831 (1967).
[51] J. E. Gunn and I. Gott, J. Richard, Astrophys. J. **176**, 1 (1972).
[52] K. Ichiki and M. Takada, Phys. Rev. D **85**, 063521 (2012).
[53] C. Wagner, F. Schmidt, C.-T. Chiang, and E. Komatsu, J. Cosmol. Astropart. Phys. 08 (**2015**) 042.
[54] V. Springel, Mon. Not. R. Astron. Soc. **364**, 1105 (2005).
[55] R. Scoccimarro, Mon. Not. R. Astron. Soc. **299**, 1097 (1998).
[56] M. Crocce and R. Scoccimarro, Phys. Rev. D **73**, 063519 (2006).
[57] T. Nishimichi, A. Shirata, A. Taruya, K. Yahata, S. Saito, Y. Suto, R. Takahashi, N. Yoshida, T. Matsubara, N. Sugiyama *et al.*, Publ. Astron. Soc. Jpn. **61**, 321 (2009).
[58] P. Valageas and T. Nishimichi, Astron. Astrophys. **527**, A87 (2011).
[59] A. Lewis, A. Challinor, and A. Lasenby, Astrophys. J. **538**, 473 (2000).
[60] Planck Collaboration, P. A. R. Ade, N. Aghanim, M. Arnaud, M. Ashdown, J. Aumont, C. Baccigalupi, A. J. Banday, R. B. Barreiro, J. G. Bartlett *et al.*, Astron. Astrophys. **594**, A13 (2016).
[61] R. E. Angulo and A. Pontzen, Mon. Not. R. Astron. Soc. **462**, L1 (2016).
[62] F. Villaescusa-Navarro, S. Naess, S. Genel, A. Pontzen, B. Wandelt, L. Anderson, A. Font-Ribera, N. Battaglia, and D. N. Spergel, Astrophys. J. **867**, 137 (2018).

[63] R. W. Hockney and J. W. Eastwood, *Computer Simulation Using Particles* (McGraw-Hill, New York, 1981).
[64] F. Bernardeau, S. Colombi, E. Gaztañaga, and R. Scoccimarro, Phys. Rep. **367**, 1 (2002).
[65] R. Takahashi, Prog. Theor. Phys. **120**, 549 (2008).
[66] T. Nishimichi and P. Valageas, Phys. Rev. D **90**, 023546 (2014).
[67] A. Taruya, Phys. Rev. D **94**, 023504 (2016).
[68] A. J. S. Hamilton, P. Kumar, E. Lu, and A. Matthews, Astrophys. J. Lett. **374**, L1 (1991).
[69] J. A. Peacock and S. J. Dodds, Mon. Not. R. Astron. Soc. **267**, 1020 (1994).
[70] B. Jain, H. J. Mo, and S. D. M. White, Mon. Not. R. Astron. Soc. **276**, L25 (1995).
[71] B. Jain and E. Bertschinger, Astrophys. J. **456**, 43 (1996).
[72] T. Nishimichi, F. Bernardeau, and A. Taruya, Phys. Rev. D **96**, 123515 (2017).
[73] M. Sato, T. Hamana, R. Takahashi, M. Takada, N. Yoshida, T. Matsubara, and N. Sugiyama, Astrophys. J. **701**, 945 (2009).
[74] M. Takada and B. Jain, Mon. Not. R. Astron. Soc. **395**, 2065 (2009).
[75] I. Kayo, M. Takada, and B. Jain, Mon. Not. R. Astron. Soc. **429**, 344 (2013).
[76] A. Taylor, B. Joachimi, and T. Kitching, Mon. Not. R. Astron. Soc. **432**, 1928 (2013).
[77] R. Takahashi, T. Nishimichi, M. Takada, M. Shirasaki, and K. Shiroyama, Mon. Not. R. Astron. Soc. **482**, 4253 (2019).
[78] A. Cooray and R. Sheth, Phys. Rep. **372**, 1 (2002).
[79] C.-T. Chiang, C. Wagner, F. Schmidt, and E. Komatsu, J. Cosmol. Astropart. Phys. 05 (**2014**) 048.
[80] J. F. Navarro, C. S. Frenk, and S. D. M. White, Astrophys. J. **462**, 563 (1996).
[81] P. S. Behroozi, R. H. Wechsler, and H.-Y. Wu, Astrophys. J. **762**, 109 (2013).
[82] W. H. Press and P. Schechter, Astrophys. J. **187**, 425 (1974).
[83] R. K. Sheth and G. Tormen, Mon. Not. R. Astron. Soc. **329**, 61 (2002).
[84] J. Tinker, A. V. Kravtsov, A. Klypin, K. Abazajian, M. Warren, G. Yepes, S. Gottlöber, and D. E. Holz, Astrophys. J. **688**, 709 (2008).